The rise and fall of Alaska glaciers detected by TOPEX/Poseidon and Jason-2 altimeters

Yung-Sheng Cheng[1], Delong Tao[2], Cheinway Hwang[3], Wenke Sun[2], and Hyongki Lee[4]

[1]Feng Chia University
[2]University of Chinese Academy of Sciences
[3]National Yang Ming Chiao Tung University
[4]University of Houston

November 23, 2022

Abstract

Satellite radar altimeters have been used to monitor sea level changes and ice sheet elevation changes for more than 3 decades. Over mountain glaciers, radar altimetry has limited applications due to contaminated radar waveforms caused by complex glacier surfaces and steep terrains. In this study, we develop a glacier-threshold method (GTM) to determine glacier elevation changes over mountain glaciers in Alaska. The GTM can detect and remove invalid elevation observations from the TOPEX/Poseidon (T/P) and Jason-2 (J2) altimeters, creating usable elevation observations from 16–92% of the raw observations. The selected elevations are used to construct long-term time series of Alaskan glacier elevation changes over 1993–2002 (T/P) and 2008–2016 (J2) at 47 sites. A crossover analysis and a Lidar comparison confirm the result from T/P and J2. Our finding shows that most of the Alaskan glaciers studied have continued to decline in recent years. The largest declining rate is -11.06 ± 0.35 m/yr over Klutlan Glacier, followed by Chitina Glacier at -8.82 ± 0.12 m/yr. Glacier thickening occurred in some accumulation zones, such as Hubbard Glacier and Logan Glacier, and also at some glacier terminuses. The mechanisms of these elevation changes are discussed using climate datasets. It is suggested that changes in environmental factors such as precipitation, air temperature and sea water temperature influence the shifts in the trends of glacier elevation changes. A sophisticated processing system and altimeter data from repeat missions can facilitate long-term monitoring of small-scaled glaciers for a better understanding of glacier dynamics.

The rise and fall of Alaska glaciers detected by TOPEX/Poseidon and Jason-2 altimeters

Yung-Shen Cheng[1,2], Delong Tao[3], Cheinway Hwang[1], Wenke Sun[3], and Hyongki Lee[4]

[1]Department of Civil Engineering, National Chiao Tung University, 1001 Ta Hsueh Road, Hsinchu 300, Taiwan

[2]Water Resources Development Center, Feng Chia University, Taichung, Taiwan

[3]Key Laboratory of Computational Geodynamics, University of Chinese Academy of Sciences, Beijing 100049, China

[4]Department of Civil and Environmental Engineering, University of Houston, 5000 Gulf Freeway, Houston, TX 77204-5059, USA

Correspondence to:

Cheinway Hwang, cheinway@nycu.edu.tw; cheinway@gmail.com

Key Points:

- Alaska glacier elevation changes are generated from TOPEX/Poseidon and Jason-2 altimeter observations and by a glacier-threshold method
- The rates of time-lapsed glacier elevations during 1993–2016 were largely negative, but some rates were positive, depending on regions
- Topography, regional environmental setting and Pacific decadal oscillation may lead to Alaska's heterogenous glacier elevation changes

Abstract

Satellite radar altimeters have been used to monitor sea level changes and ice sheet elevation changes for more than 3 decades. Over mountain glaciers, radar altimetry has limited applications due to contaminated radar waveforms caused by complex glacier surfaces and steep terrains. In this study, we develop a glacier-threshold method (GTM) to determine glacier elevation changes over mountain glaciers in Alaska. The GTM can detect and remove invalid elevation observations from the TOPEX/Poseidon (T/P) and Jason-2 (J2) altimeters, creating usable elevation observations from 16–92% of the raw observations. The selected elevations are used to construct long-term time series of Alaskan glacier elevation changes over 1993–2002 (T/P) and 2008–2016 (J2) at 47 sites. A crossover analysis and a Lidar comparison confirm the result from T/P and J2. Our finding shows that most of the Alaskan glaciers studied have continued to decline in recent years. The largest declining rate is -11.06 ± 0.35 m/yr over Klutlan Glacier, followed by Chitina Glacier at -8.82 ± 0.12 m/yr. Glacier thickening occurred in some accumulation zones, such as Hubbard Glacier and Logan Glacier, and also at some glacier terminuses. The mechanisms of these elevation changes are discussed using climate datasets. It is suggested that changes in environmental factors such as precipitation, air temperature and sea water temperature influence the shifts in the trends of glacier elevation changes. A sophisticated processing system and altimeter data from repeat missions can facilitate long-term monitoring of small-scaled glaciers for a better understanding of glacier dynamics.

Plain Language Summary

Satellite radar altimetry is an important observation technology to determine changes in surface elevations. However, altimeter measurement accuracy is very sensitive to terrain complexity, especially over mountain glaciers. Here we present a glacier-threshold method (GTM) to investigate the glacier elevation changes in Alaska, using TOPEX/Poseidon (T/P) and Jason-2 (J2) altimeter measurements. Internal and external accuracy assessments show the GTM enables us to retrieve precise changes in glacier elevations and improve the usable rate of original radar observations. During the recent study period, the vast majority of Alaska glaciers are rapidly declining. The maximum declining rate reached 11.06 ± 0.35 m/yr near Klutlan Glacier. But in some glacier accumulation areas and glacier tongues, the glacier elevations were rising. A climate factor analysis shows that the changes in precipitation, air temperature and sea water temperature are responsible for the asynchronously spatio-temporal glacier elevation changes. All these findings from the repeat-track radar altimetry and the GTM help to improve our knowledge about Alaska glacier processes.

Keywords: Alaska glaciers, Altimeter, Environmental change, Jason-2, TOPEX/Poseidon, Waveform retracking

1 Introduction

There are more than 10,000 glaciers in Alaska, 98% of which are retreating and thinning (*Molnia*, 2007). Glaciers in Alaska began to retreat as early as in the 18th century, and some small glaciers have disappeared in the 20th century (*Molnia*, 2008). A recent study shows that Alaska's rapidly melting glaciers contributed to one third of the global sea level rise over the past half century (*Zemp et al.*, 2019). Mass losses associated with Alaska glacier melting have been detected by the Gravity Recovery and Climate Experiment (GRACE) data. *Luthcke et al.* (2008); (2013) first used GRACE mascon solutions to confirm significant mass losses in Alaska, similar to the results from the solutions using spherical harmonic expansions (*Jacob et al.*, 2012; *Gardner et al.*, 2013; *Wouters et al.*, 2019). The latest time-varying gravity observations of GRACE and GRACE Follow-On show that the glacier-induced mass losses are intensifying with a loss rate of -72.5 ± 8 Gt/yr (*Ciracì et al.*, 2020). However, the GRACE gravimetry data over the Alaska mountain glaciers reflect only large-scale mass changes due to its coarse spatial resolution (~350 km) (*Wang et al.*, 2012). In contrast, satellite imagery can provide small-scale, two-dimensional and three-dimensional changes of mountain glaciers, which can play a critical role in quantifying glacier discharge and the mass balance here (*Berthier et al.*, 2010; *Heid and Kääb*, 2012; *Brun et al.*, 2017; *Dussaillant et al.*, 2019). However, the temporal resolution of satellite imagery can be easily altered by cloud covers, resulting in incomplete seasonal observations of glacier dynamics, and potentially incorrect long-term trends. In order to detect glacier changes at a smaller scale than GRACE, and to ensure the establishment of a continuous and robust time series, a different sensor, such as satellite altimetry, becomes necessary.

At present, there are two types of satellite altimeters, namely laser and radar altimeters. A laser altimeter, such as Ice, Cloud, and land Elevation Satellite (ICESat), has a small illuminating footprint of about 70 m, which is less affected by rough terrains compared to radar altimeters. The ICESat altimeter can measure glacier heights at a near-repeat spot for about 3–4 times a year, but only limited observations has been made over Alaska (*Muskett et al.*, 2008). *Kääb et al.* (2012) measured the variations in mountain glacier elevations over the Himalayas using ICESat. *Gardner et al.* (2013) estimated glacier mass changes using ICESat and showed the contribution of global glacier melting to sea level rise. Current studies using GRACE or ICESat showed that most mountain glaciers in Alaska were melting during 2003–2009. ICESat-2, launched in 2018, continues ICESat observations to extend the elevation records of global glaciers (*Neumann et al.*, 2019). Despite the high-accuracy heights in mountainous areas from ICESat/ICESat-2, the rates of glacier elevation change estimated from the two altimeters still contain large uncertainties due to their non-repeat ground tracks.

An altimeter with an exact repeat orbit (but subject to roughly 1-km offset relative to the nominal orbit) is typical for oceanographic applications. Examples of exact-repeat altimeters are Geosat, ERS-series of altimeters and TOPEX/Poseidon (T/P)–series of altimeters. The T/P-series altimeters include the T/P, Jason-1, 2 and 3 altimeters, which measure surface elevations along their repeated ground tracks every 10 days. In theory, the exact-repeat radar altimeters can provide long-term and continuous observations for glacier monitoring. However, radar altimeters have much larger footprints than those of ICESat/ICESat-2, despite the recent improvement using the delay Doppler technique (*Raney*, 1998) that can result in a 300-m resolution in the along-track direction (*McMillan et al.*, 2019). Such large footprints make most radar-based altimeters difficult to observe precise elevations over mountain glaciers, where the terrain can be rugged and sloping, and radar signals can suffer from volume scattering and radar penetration (*Lee et al.*, 2013). These surface conditions over glaciers can contaminate radar waveforms to result in low-precision range measurements over mountain glaciers. Retrackers for remedying contaminated waveforms include offset center Gravity retracker (*Wingham et al.*, 1986), beta retracker (*Martin et al.*, 1983), ICE-2 retracker (*Legresy and Remy*, 1997), threshold retracker (*Davis*, 1997), modified threshold retracker (*Lee et al.*, 2008) and sub-waveform threshold retracker (*Yang et al.*, 2012). Improved radar ranges over glaciers have been used to calculate glacier heights and their changes (*Wingham et al.*, 2009; *Lee et al.*, 2013; *Forsberg et al.*, 2017). In particular, *Lee et al.* (2013) showed that the glacier elevation change from T/P and Envisat are able to detect the 1993–1995 and 2008–2011 surge events over Alaska glaciers.

The objective of this paper is to demonstrate the implementation of a glacier-threshold method (GTM) to generate precise elevation measurements from T/P and J2 radar altimeters, then detect and analyze trends of elevation change of glaciers at 47 sites (Figure 1 and Table A1) in Alaska. This paper is organized as follows. Section 2 shows the satellite altimetry data, airborne Lidar data and the digital elevation model (DEM). Section 3 presents the GTM and demonstrates the method step by step. Section 4 shows the long-term glacier elevation changes detected by GTM, which are then verified and analyzed, taking into account the impact of regional Alaska environmental factors on glacier changes. Section 5 concludes this study.

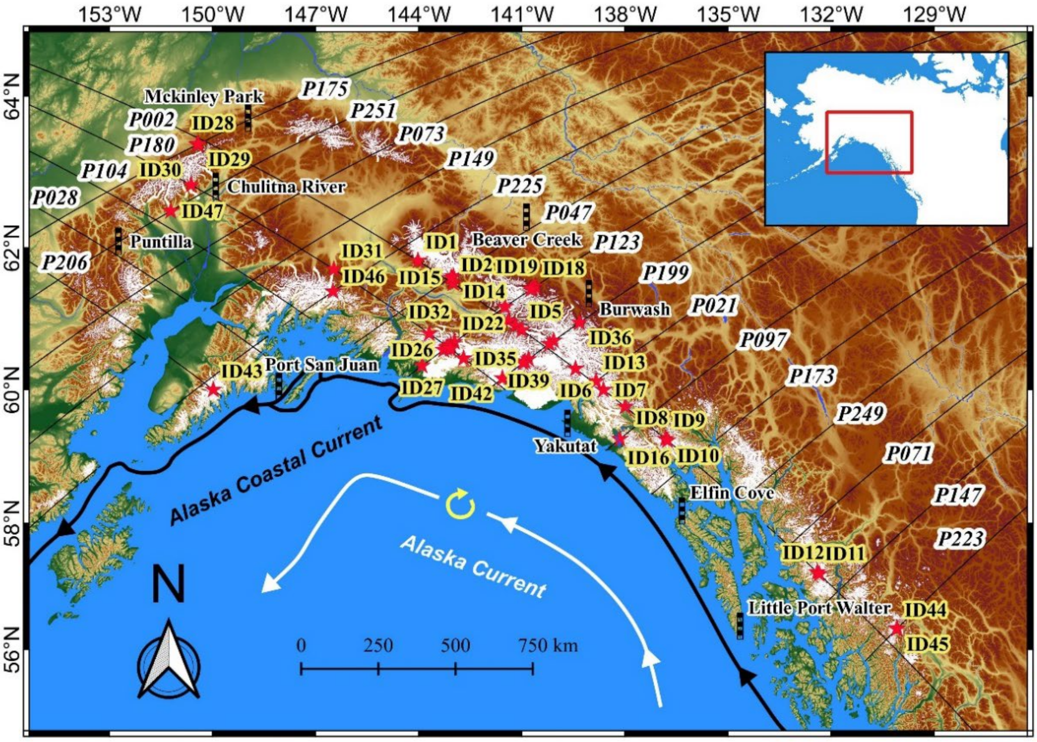

Figure 1. Ground tracks (black fine lines) of T/P and J2 over Alaska glaciers, with the pass numbers (P). An ID is a glacier site with elevation changes from the altimeters. Here only selected glacier IDs are shown (see Table A1 for the full list of glacier names, longitudes, latitudes and elevations).

2 Data

2.1 TOPEX/Poseidon and Jason-2 altimeter data

The main measurements to detect elevation changes over Alaska mountain glaciers are T/P and J2. T/P and J2 belong to a family of radar altimeters, and repeat the same ground tracks every 10 days on 254 passes. Figure 1 shows the ground tracks of the 21 passes of the two satellites. Each of the T/P data records contain 10-Hz elevation measurements, spaced at an interval of 660 m. The orbit heights, range measurements, and geophysical corrections were acquired from the geophysical data records (GDRs), and 64-sample radar waveforms are acquired from the sensor data records (SDRs). Following the approach of *Lee* (2008), we re-sampled the original 128 waveforms of T/P into 64 waveforms for retracking. The T/P mission lasted from October 1992 through August 2002 (cycles 1–364). Unlike T/P, the J2 dataset contains 20-Hz measurements, corresponding to an interval of 330 m. The orbit heights, range measurements, geophysical corrections, and the 104-sample waveforms were acquired from sensor geophysical data records (SGDRs).

Due to the design of the Jason-1 satellite radar altimeter, and several problems in data processing, the elevation measurements of Jason-1 over land are not usable (*Frappart et al.*, 2006; *Hwang et al.*, 2016). Therefore, we only used the measurements from T/P and J2. Jason-3 are not used because of the limited time of research. The altimeter-derived elevation time series span two periods: 1992-2002 (T/P) and 2008-2016 (J2). Over Alaska's mountain glaciers, the wet tropospheric delays were corrected using the European Center for Medium-Range Weather Forecasts (ECMWF) model. All the altimeter data used in this paper were downloaded from the web site of the French Archiving, Validation and Interpretation of Satellite Oceanographic data (AVISO) at http://www.aviso.altimetry.fr/.

2.2 IceBridge UAF Lidar data

We used airborne Lidar datasets to verify the altimeter-derived Alaskan glacier elevation time series. The Lidar dataset is obtained from the Airborne University of Alaska Fairbanks (UAF) Glacier

Lidar System and contains surface elevations of Alaskan glaciers. The dataset is a result from the NASA Operation IceBridge program. The Lidar observations were collected using laser ranging to glacier surfaces on a fixed wing aircrafts that was positioned by the Global Positioning System with attitude corrections from the inertial measurement unit (GPS/IMU) (*Larsen*, 2010). The footprint of a laser pulse is about 20 centimeters in diameter. The average along-track and cross-track spacings are 1 m by 1 m. The average accuracy of the elevation measurements is better than 30 cm. We used high-resolution and high-precision repeated elevation observations from this dataset to assess our altimeter result. The web site of the Lidar data is https://nsidc.org/data/ILAKS1B/versions/1.

2.3 Digital elevation model

A digital elevation model (DEM) is needed when applying the GTM method in this paper. The DEM was used to correct for the terrain gradient effect and remove erroneous land surface heights (LSH) from the altimeters. The DEM used in this paper is from SRTM_plus (*Becker et al.*, 2009), which is on a 15″×15″ grid. This DEM was constructed from the measurements of the Shuttle Radar Topography Mission (SRTM), augmented by elevation data from other satellite missions. Note that there are several versions of DEM from SRTM with the finest spatial resolution being 3″×3″ (90 m). However, the SRTM DEMs provide elevations only within latitudes ± 55° without covering Alaska mountain glaciers (> 55°N). To use a unified DEM, we decided to choose the SRTM_plus DEM. We converted the elevations from T/P and J2 to the elevations with respect to the WGS84 ellipsoid (used by the SRTM_plus), based on the differences in the ellipsoidal parameters for T/P and the WGS84. The SRTM_plus DEM was downloaded from ftp://topex.ucsd.edu/pub/srtm15_plus/.

3 Methods

A radar altimeter can measure precise glacier elevations over flat, open areas in polar ice sheets, but not in mountain glaciers without careful data processing. In the study, we present the glacier-threshold method (GTM) to generate robust glacier elevation changes over Alaska mountain glaciers.

The procedure of the GTM for T/P and J2 data is shown in Figure 2. Some of the steps in the procedure were shown in (*Hwang et al.*, 2021). To avoid repetitions, the steps given by (*Hwang et al.*, 2021) will only be briefly described in the following subsections. The five steps in the GTM are:

a) Determine the optimal waveform retracking algorithm to retrack waveforms;
b) Select valid altimetry observations;
c) Correct terrain slope and terrain gradient effect;
d) Calculate the linear trend of each site laying on glaciers;
e) Assess the detected elevation change by crossover analysis.

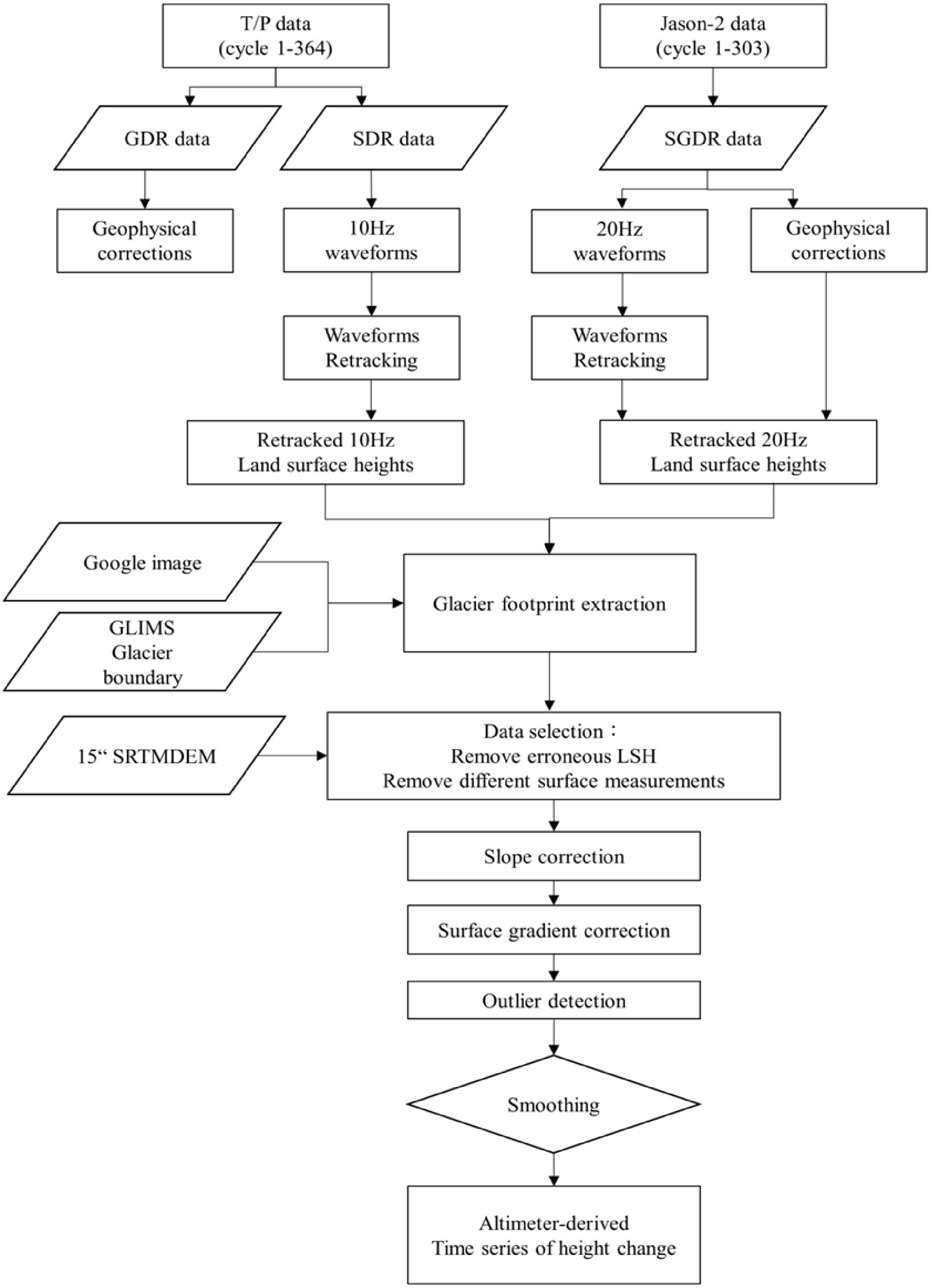

Figure 2. Flowchart of the GTM for retrieving precise glacier elevation changes.

3.1 Waveform Retracking

The glacier elevation ($H_{glacier}$) from altimeter measurements at a given nadir point can be expressed as:

$$H_{glacier} = H_{sat} - H_{alt} - H_{cor} - H_{terrain} - H_{retrack} \quad (1)$$

where $H_{glacier}$ is the height of glacier; H_{sat} is the satellite altitude; H_{alt} is the range measurement (for T/P and J2); H_{cor} is the integration of geophysical corrections (in the GDR product of the T/P satellite and the SGDR product of the Jason-2); $H_{terrain}$ is the terrain correction, which will be described in subsection 3.4; $H_{retrack}$ is the range correction from waveform retracking.

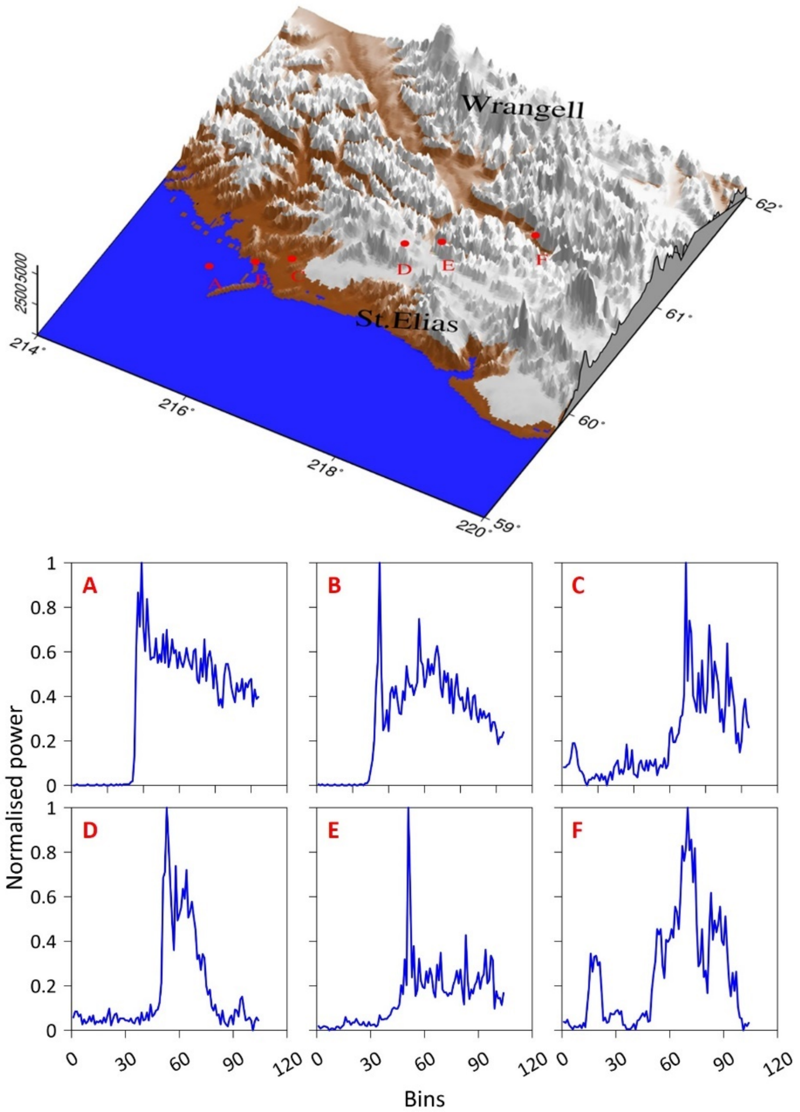

Figure 3. Glaciers over Alaska (top, white-shaded areas) and radar altimeter waveforms A-F over different surface types along pass 123 of J2.

Altimeter radar waveform retracking is an important part for generating precise range measurements from complex waveforms. A radar altimeter generated returned waveforms from the reflecting radar pulses to determine the two-way travel times for range measurements. Over a rough or uneven land surface, returned waveforms of radar altimeters can be different from the default Brown model (*Brown*, 1977). Figure 3 shows sample J2 waveforms along pass 123 over six different types of surfaces in Alaska: ocean (A), coastal area (B), flat terrain(C), ice (D), steep slope (E), and complex terrain (F, mixed rock and ice). The waveform the ocean surface is the closest to the Brown model (see waveform A in Figure 3). As the altimeter approaches land from the oceans, the waveforms become irregular due to waveform contamination. In particular, the waveforms become more complex over rough ice surfaces (see waveform D and F in Figure 3) or steep-sloped terrains (see waveform E in Figure 3).

We retrack waveforms to detect the gates of the actual midpoint of the waveform leading edge to correct for range errors over Alaskan mountain glaciers. For a given waveform, range correction from waveform retracking is:

$$H_{retrack} = (G_r - G_t) \times 0.46875 \quad (2)$$

where G_r is the retracked gate, G_t is the default tracking gate (the default is 24.5 and 32.5 for T/P and J2, respectively, unitless), and 0.46875 m is the length of a gate for the Ku-band altimeter.

Several algorithms for waveform retracking can improve the precision of radar range measurement, such as off-center of gravity (*Wingham et al.*, 1986), the threshold algorithm (*Davis*, 1997), and the Sub-waveform algorithm (*Yang et al.*, 2012). To determine the optimal algorithm of waveform retracking in this study, we experimented with these three algorithms (including various threshold values) for waveform retracking. The best retracker used in this paper is described and assessed in Section 3.5.

Table 1. Rates of glacier elevation change (in m/yr) from J2 data at the crossover of passes 123 and 180 from different retracking methods

Retracking algorithm	Pass		Difference
	123	180	
OCOG	-2.54	-1.88	0.66
Threshold（50%）	-2.47	-1.72	0.75
Sub-waveform（10%）	-1.87	-1.56	0.31
Sub-waveform（20%）	-2.18	-1.8	0.38
Sub-waveform（30%）	-1.5	-1.7	0.2
Sub-waveform（50%）	-1.57	-1.56	0.01

3.2 Altimeter data selection

Selecting usable waveforms and retracking them for precise elevations is a crucial part of the GTM. We follow the selection criteria presented in (*Hwang et al.*, 2021) to select the needed waveforms. The waveforms over Alaska glaciers are specular like the D waveform in Figure 3, consistent with the view of *Lee* (2008) and other studies over ice sheets and glaciers. A returned waveform is not only related to characteristics of the radar-illuminated surface, but also to the distance between the radar altimeter and the surface. Over ice surfaces, the automatic gain control (AGC) onboard T/P and J2 can theoretically help to maintain suitable returned powers (*Fu and Cazenave*, 2000), but the AGC cannot guarantee preventing the return powers from becoming fully saturated. *Hwang et al.* (2016) showed that the range errors can reach 100 m if altimeter radar waveforms were damaged by complex surface.

Therefore, we first identify whether altimetry footprints are over glaciers by using Global Land Ice Measurements from Space (GLIMS) and Google Earth images. The criterion for the identification is that the measurements are within the polygons of glaciers defined by GLIMS and also over an ice/snow surface on Google Earth images. We then classify the waveforms to identify valid waveform measurements and for each waveform we computed the peak power of waveform, and removed the value of peak power smaller than 1.8. More details can be found in *Peacock and Laxon* (2004), *Lee* (2008), and *Yang et al.* (2012). Additionally, we applied a cluster analysis method and the algorithm of *Dabo-Niang et al.* (2007) to distinguish between useful and bad waveforms. But it turns out that glacier heights corrected by waveform retracking cannot automatically yield useful time series of glacier elevation change without further data screening. Therefore, we used the SRTM_plus DEM to remove outliers of measurement over mountain glaciers: The LSH is regarded as an outlier when the difference between the LSH and the DEM elevation exceeds 150 m (*Hwang et al.*, 2021).

It is challenging to obtain precise LSHs from radar altimeters over steep slopes due to high uncertainty (*Brenner et al.*, 2007), and the rate of elevation change is not consistent at different altitudes. For example, over the Greenland Ice sheet, the elevation changes from the Envisat altimeter (2002-2010) varied with altitude. The results represent positive trend in high altitude area, and represent negative trend in low altitude area (*Forsberg et al.*, 2017). Thus, for a given site in this paper we used 15″×15″ SRTM to select suitable altimeter measurements in a bin with a 1-km radius, centered at the location of a reference point. The reference point is determined by individual inspections of all sites. In this step, the altimeter measurements falling into the 100 m contour (like the red points in Figure 4) are candidate measurements for a bin. Figure 4 shows an example of how altimetry measurements are selected over different altitudes (black points) in a bin.

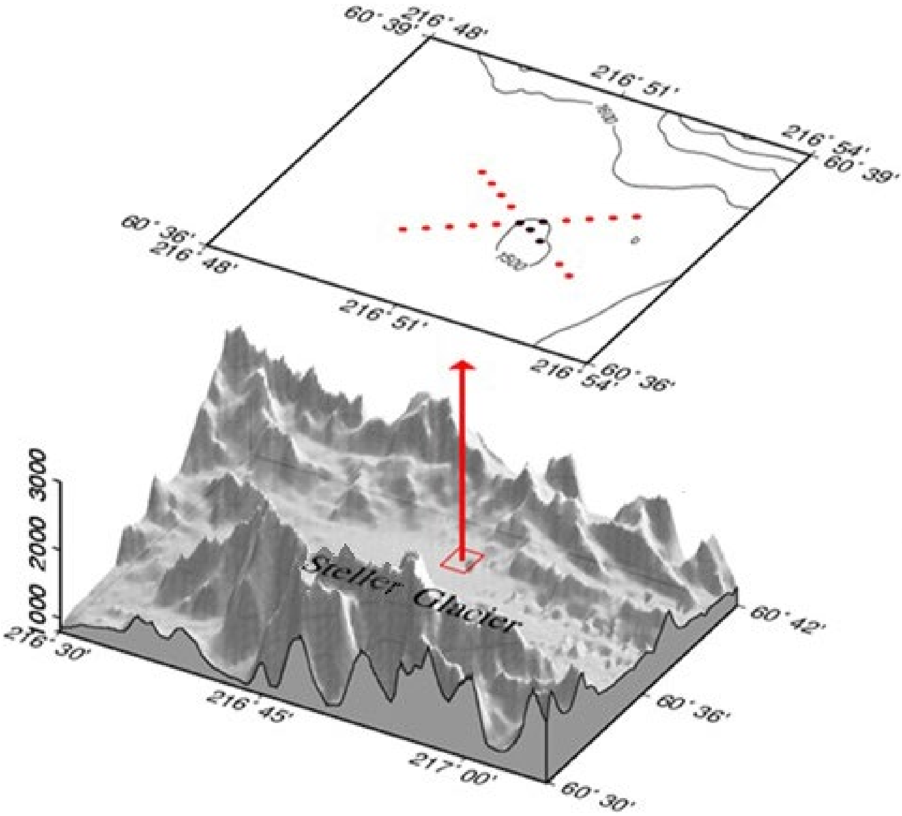

Figure 4. An example showing selected altimeter measurements (red dots) from J2 around Sites 24 and 33 (see Table A1 for coordinates) near the crossover of passes 123 and 180. The selected measurements have elevations ranging from 1500 to 1600 m over a gently sloping glacier surface, where the effects of lateral offset in repeated tracks and terrain gradient can be reliably corrected. Compared to a rugged surface, the measurements at the black points are over steep slopes (rugged terrain) and thus are excluded.

3.3 Correction for terrain effect

Corrections for terrain effect include the slope correction and terrain gradient correction. The slope-induced error is caused by the difference between sub-satellite point and the closest point on a sloping surface (*Brenner et al.*, 1983). The terrain gradient error due to the lateral shift of repeated tracks in the cross-track direction (about ± 1 km). Below we show how these corrections are applied.

(a) Outlier removal, elevation adjustment

First, we fitted the following least-squares model to the selected measurements from repeat cycles at a bin (*Hwang et al.*, 2021):

$$\begin{aligned} H_i^j(\varphi,\lambda,t) + v_i^j \quad = \quad & a_0 + a_1(t-t_0) + a_2(\varphi-\varphi_0) + a_3(\lambda-\lambda_0) + \\ & a_4(\varphi-\varphi_0)^2 + a_5(\lambda-\lambda_0)^2 + a_6(\varphi-\varphi_0)(\lambda-\lambda_0) \end{aligned} \tag{3}$$

where $H_i^j(\varphi,\lambda,t)$ is the LSH from altimeter at geodetic latitude (φ), longitude (λ), and measured time (t), included range correction from waveform retracking, *j* is the repeat cycle, *i* is the *i*th measurement from repeat cycle *j* at this bin, v_i^j is the residual of $H_i^j(\varphi,\lambda,t)$, φ_0 and λ_0 represent the location of reference point in this bin, a_0 is the mean height at this bin, a_1 is the initial rate of elevation change, a_2, a_3, a_4, a_5 and a_6 are coefficients of 2^{nd} order surface fitting from all repeat cycles at this bin.

In the least-squares adjustment, the weight of an observation is the inverse distance between the measurement point and reference point. After the first-round of adjustment, the residuals (v_i^j) for all measurements and the a posteriori variance of unit weight is computed. If a residual (v_i^j) is two times larger than the squared root of the a posteriori variance, we need to remove the corresponding measurement and perform the next-round of adjustment without the removed measurements and stop the adjustment when no measurements are removed. According to *Flament and Rémy* (2012), the coefficients of 2^{nd} order surface can reduce the effects of terrain. More details of the coefficients of 2^{nd} order surface also can be found in *Remy and Parouty* (2009) and Hwang et al. (2021). An adjusted, outlier-free elevation can be expressed as:

$$\hat{H}_i^j(\varphi,\lambda,t) = H_i^j(\varphi,\lambda,t) + v_i^j \tag{4}$$

(b) Correction for lateral offset of ground track

As mentioned earlier, the actual tracks of the satellite do not repeat exactly. This can introduce the terrain gradient effect. Before retrieving glacier elevation changes at each site, the along-track heights should be reduced to the heights along reference tracks. Here, we use a 15′′×15′′ SRTM to correct the terrain gradient as (*Lee*, 2008):

$$H_i^j(\varphi_0,\lambda_0,t) = \hat{H}_i^j(\varphi,\lambda,t) + DEM(\varphi_0,\lambda_0) - DEM(\varphi,\lambda) \tag{5}$$

where $H_i^j(\varphi_0,\lambda_0,t)$ is the *i*th LSH after terrain gradient correction at reference point (φ_0,λ_0) from repeat cycle *j* in this bin, $DEM(\varphi_0,\lambda_0)$ and $DEM(\varphi,\lambda)$ are the elevations from the 15″×15″

DEM at the reference point and the observation point.

3.4 Altimeter-derived elevation changes

After the elevation measurements from all cycles in a bin were treated using the methods described in Section 3.2-2.4, for each cycle we averaged the measurements to form a representative height:

$$\bar{H}^j(\varphi_0, \lambda_0, t) = \frac{\sum_{i=1}^{n} H_i^j(\varphi_0, \lambda_0, t)}{n} \tag{6}$$

where $\bar{H}^j(\varphi_0, \lambda_0, t)$ is the representative height at reference point (φ_0,λ_0) for cycle j, n is the number of measurements in the bin.

In order to reduce high-frequency noises, a Gaussian filter was used to smooth the time series of glacier elevation change. Then, we compute the trend of elevation changes at (φ_0, λ_0) from the altimeter-derived time series by the model as follows:

$$\Delta\bar{H}^j(\varphi_0, \lambda_0, t) = a + bt + c\,cos(2\pi\omega t) + d(2\pi\omega t) \tag{7}$$

where $\Delta\overline{H^j}(\varphi_0, \lambda_0, t)$ is the altimeter-derived elevation change of mountain glacier, t is the time relative to the average time, a is the mean, b is a linear trend (rate of elevation change), $\sqrt{c^2 + d^2}$ is the amplitude of the annual oscillation, and ω is the annual frequency (one cycle per year).

A robust least-squares method is used to estimate the four parameters (a, b, c, and d), with equal weights for all measurements. We also estimated the uncertainty of rate (b) in Eq. 7. In this paper, an estimated rate of elevation change is accepted only when it meets the following two criteria: 1) The absolute value of elevation change rate is larger than its standard error; 2) The ratio between the number of elevation measurements in a time series and the number of all cycles is larger than 15% (see column 3 of Table A2 and Table A3). This ratio is also defined as the usable data percentage in this study.

3.5 Method validation by an internal accuracy assessment at a crossover

Due to a lack of in situ glacier elevation measurements (such as elevations from GPS, total station and Lidar observations), it is challenging to assess the uncertainties of elevation changes from T/P and

J2 over Alaska glaciers. Here, we use a crossover analysis to assess the “internal” accuracies of elevation changes from the T/P and J2 altimeters. An external accuracy analysis using Lidar measurements is made in Section 4.1. The selected crossover point is at the intersection of pass 123 (ascending track) and pass 180 (descending track), located around ID 24 and ID 33 (Figure 1 and Table A1). Here, we compare two time series of glacier elevation change from pass 123 and 180. We experimented with different waveform retracking algorithms to obtain different elevation change rates at this crossover point. As shown in Table 1, the sub-waveform algorithm with a 50-% threshold results in a minimum difference between the elevation change rates from pass 123 and 180.

Figure 5a and b compares the time series from T/P and J2 for pass 123 and 180, resulting from the use of the sub-waveform retracker with a 50-% threshold value. From the T/P data (1992–2002), the difference between the rates from the two passes is 0.21 m/yr and the difference is 0.01 m/yr from the J2 data (2008–2016). The patterns of elevation change from pass 123 and 180 at this crossover are consistent, despite some differences in the two time series. These differences may be caused by spatial and temporal factors, such the 2-day difference between the time of measurement from 123 and that from 180. Another explanation may be that the automatic gain control (AGC) reacted to the surface elevations differently for pass 123, which traveled from ocean to land pass and for pass 180, which traveled from land to ocean.

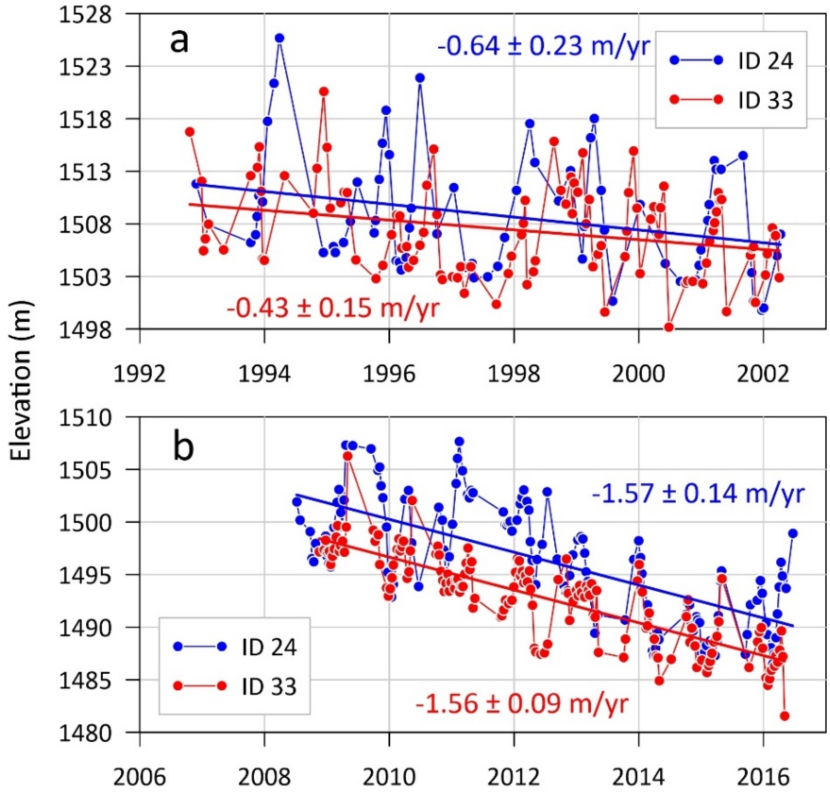

Figure 5. (a) The time series of glacier elevation change and their rates from T/P data at the crossover point, corresponding to ID 24 if data from pass 123 are used (blue dots), to ID33 if data from pass 180 are used (red dots), **(b)** same as (a), but from J2 data. The elevations are corrected by the sub-waveform retracking with a 50% threshold (Table 1).

4 Results and Discussion

4.1 External assessment using Lidar measurements

An external accuracy assessment of the glacier elevation changes determined in this study is made using the airborne Lidar data described in Section 2.3. In order to avoid the impact of the systematic bias between the Lidar measurements and the altimeter measurements (J2 only), we calculated the differences of elevations detected by the two kinds of sensors, named D_L (the difference of the elevations at a spot from the two airborne Lidar surveys) and D_{J2} (similar to D_L, but from J2 with a slightly different time span). At a given site, the D_L and D_{J2} value and their associated time spans can be used to compute the rates of elevation change in the respective time spans (the time spans are nearly the same), and the difference between the two rates is called D_r. At a given site, the elevation from

Lidar is defined as the mean of the elevations within a radius of 300 m to the site (*Trantow and Herzfeld*, 2016), and the elevation from J2 is obtained by spline interpolation from the J2-derived time series. Due to the rapid seasonal and interannual changes of glaciers, only the sites with dense and robust time series of J2 are used for comparison with the Lidar measurements. Ultimately, we selected seven sites (ID 4, 5, 18, 20, 31, 37 and 47) over six glaciers (Walsh, Logan, Klutlan, Tazlian, Hubbard and Kahiltna Glacier) for this comparison.

Table 2 shows the values of D_L, D_{J2} and D_r at the seven sites. From Table 2, in general the patterns (signs) of the glacier elevation changes from Lidar (D_L) and J2 (D_{J2}) at each site are consistent, but with varying discrepancies from one site to another. At Site 31 and Site 47, the D_r values are the smallest because of the stable change of glaciers, dense time series of J2, and the flat terrains at these sites. The largest D_r (absolute value) occurs at Site 5, followed by Sites 4, 18 and 20. Because the time spans for each D_L and D_{J2} are only slightly different, temporal glacier variabilities around the sites with large differences (D_r values) are unlikely to be a dominant for the large differences. Table 2 shows the D_r values are correlated with the slopes. This correlation may result from relatively large uncertainties in the Lidar and J2 elevation measurements over glaciers with large slopes. In general, the Lidar elevation measurements confirm the elevation changes from J2, but the result in Table 2 shows a mean discrepancy of 1.15 m/yr (average of absolute D_r) and a standard deviation of 0.84 m/yr in the differences of the rates from Lidar and J2 at the seven sites. Both the Lidar and J2 measurements show rising glacier elevations at Site 37, despite a discrepancy in the two rates. At Site 5, the rate of elevation change from Lidar is -20.22 m/year, compared to -12.48 m/year from J2. Thus, both Lidar and J2 show large glacier elevation drops near Site 5 in the 2010s.

Table 2. A comparison of differenced heights and resulting rate difference at 7 sites

Site ID	Pass	Period	D_L (m)	D_{J2}(m)	Dr (m/yr)	Slope (°)
ID 4	2	2015/08 – 2016/08	-3.77	-5.32	-1.67	0.9
ID 5	2	2013/08 – 2016/08	-20.22	-12.48	2.64	3.1
ID 18	123	2013/08 – 2014/08	-8.84	-12.21	-1.67	1.2
ID 20	123	2013/08 – 2014/08	-9.21	-11.55	-1.16	0.5
ID 31	180	2009/08 – 2012/03	-1.23	-1.94	-0.28	0.5
ID 37	199	2011/08 – 2014/05	1.72	0.28	-0.52	0.5
ID 47	251	2010/05 – 2013/05	-4.59	-5.02	-0.14	0.1

4.2 Patterns of glacier elevation changes from T/P and J2

The T/P and J2 altimeter observations spanned nearly two decades (from January 1993 to 2016 in this paper), resulting in various patterns of glacier changes over Alaska. Here we classify the 47 sites to three categories of patterns: (I) those with similar trends in glacier elevation changes with evident elevation discontinuities (Figure 6), (II) those with reverse trends and evident elevation discontinuities (Figure 7), (III) those with similar trends and no clear elevation discontinuities (Figure 8). Evident elevation discontinuities might be caused by a number of factors, including T/P-J2 inter-altimeter biases, terrain effect, and changes in climate pattern.

Previous studies showed that there are inter-altimeter biases in monitoring inland water and ocean dynamics using similar types of radar altimeters (*Beckley et al.*, 2004; 2010; *Hwang et al.*, 2016). Such systematic differences are associated with the different levels of measurement accuracy and topographic complexity. In some cases, constants were applied to correct for the biases (*Wingham et al.*, 2006; *Fricker and Padman*, 2012). However, over ice surfaces, inter-altimeter biases usually have distinct spatial patterns (*Frappart et al.*, 2016). The inter-altimeter biases of a tandem mission can be estimated through a collinear difference of simultaneous measurements at a small scale (*Wingham et al.*, 2006; *Schröder et al.*, 2019). Since J2 was launched several years after T/P and they used different altimeters, identifying range biases over glacier surfaces between them is difficult. A method based on long-term rate reference has been used to eliminate this offset (*Schröder et al.*, 2019), but the premise of a stable trend of glacier elevation change must be met. For the sites with similar trends but with evident elevation discontinuities (Figure 6), the rate-reference correction method seems feasible for bias corrections. However, the method is invalid for the sites with reverse trends and evident elevation discontinuities (Figure 7). Because of the lack of reliable reference observations, it is challenging to remove the biases between the glacier elevations from T/P and J2. Thus, we decide not to correct for any potential inter-altimeter biases between T/P and J2, and the result in this paper genuinely reflects the capabilities of T/P and J2 in observing glacier elevation changes over Alaska.

J2 obtains elevations at a frequency of 20 Hz with an along-track spacing of ~330 m, which is half that of T/P. Terrain undulations within the footprints of T/P and J2 can also cause different ranging biases that introduce elevation discontinuities between the two altimeters. Moreover, the inherent different ranging techniques of the radar altimeters used by T/P and J2 can result in different usable data rates at a given glacier site. For example, the J2 altimeter (called Poseidon-3 altimeter) used an open-loop tracker mode that can successfully track backscatter signals over rapidly varying terrains (*Martin-Puig et al.*, 2016). Furthermore, large terrain slopes can introduce greater uncertainties in the observed glacier elevation changes. In this study, the SRTM_plus was employed to reduce the error of terrain effect. The ice topography from this DEM product results from different ICESat acquisitions in different seasons and years (*Becker et al.*, 2009), and the profiles measured by ICESat represents the full topography.

During the study period (1993–2016), the changes in the rates of glacier elevation change in Figure 6, 7 and 8 may also reflect shifts in climate pattern. *Wendler et al.* (2017) showed that the Pacific Decadal Oscillation (PDO) had substantial impacts on the climate of Alaska. After 1998, the PDO has changed from a positive phase to a negative phase, leading to colder temperatures and lower precipitations. The inter-annual fluctuation in the PDO index in the negative phase has lasted for decades before the index changed from negative values to positive ones in 2014. These inter-decadal climate phase shifts occurred just across the mission period of T/P and J2 (1993–2016). More analyses about the spatially heterogeneous responses of Alaskan glaciers to PDO will be discussed in Section 4.4.

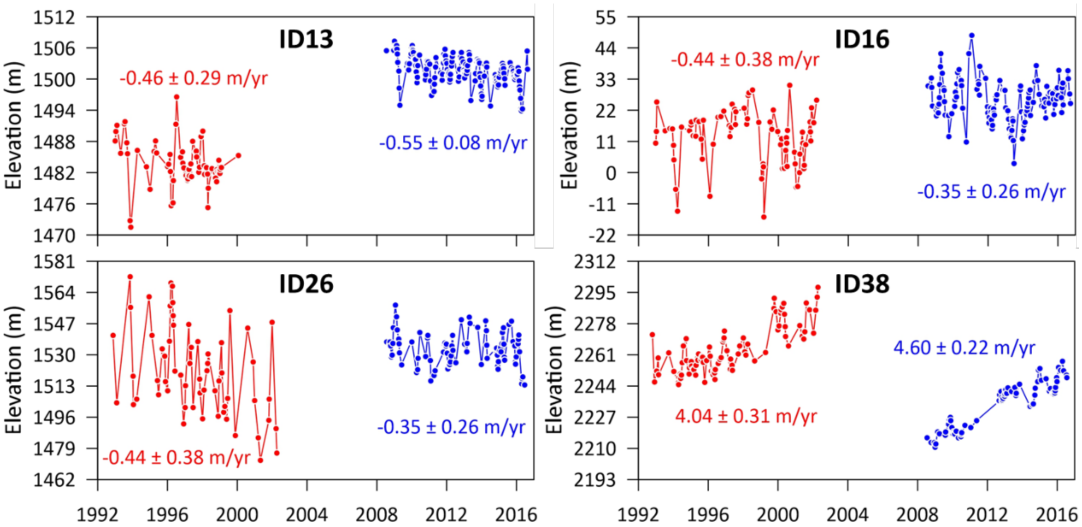

Figure 6. Glacier elevation changes at Sites 13, 16, 26 and 38, with similar trends but with evident elevation discontinuities.

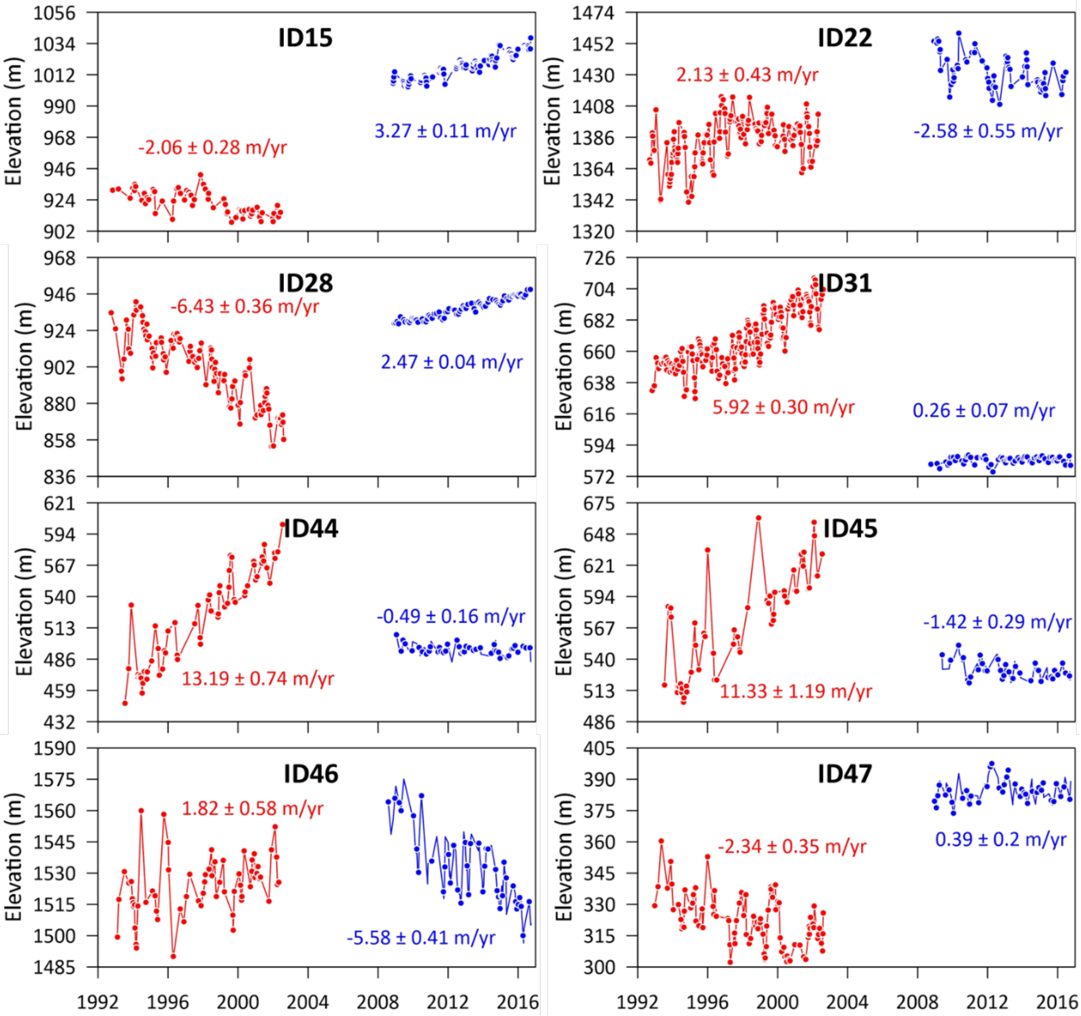

Figure 7. Glacier elevation changes at Sites 15, 22, 28, 31, 44, 45, 46 and 47, with reverse trends and evident elevation discontinuities.

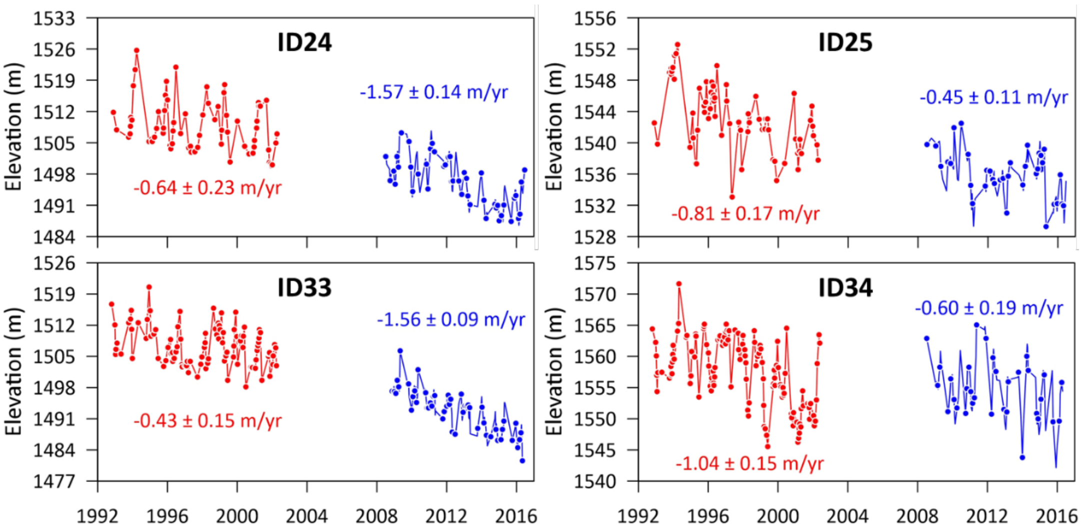

Figure 8. Glacier elevation changes at Sites 24, 25, 33 and 34 with similar declining trends and negligible elevation discontinuities.

4.3 Recent rates of Alaska glacier elevation changes from J2

Here, we discuss recent glacier elevation changes rates over Alaska glaciers using the J2 result over 2008–2016. Figure 9 shows the rates at the 47 sites from J2 given in Table A3. In total, 25 glaciers are included (Sites 24 and 33 are at a crossover point, thus the same glacier). Most sites are located in St. Elias mountains, Kenai Mountains, Chugach Range, Coast Range and Wrangell Mountains. Glaciers thinning and retreat in these regions contributed 90% of the freshwater discharge into the Gulf of Alaska (*Neal et al.*, 2010). Few sites are distributed in central Alaska range. At most sites, the glacier elevations were falling (negative rates of elevation change), but at some sites the glacier elevations experienced positive rates. The varying patterns of glacier elevation changes may be caused by glacial dynamics, atmospheric circulation and climate sensitivity (*Berthier et al.*, 2010; *Menounos et al.*, 2019). Below we analyze selected groups of glaciers to discuss such heterogeneous elevation changes.

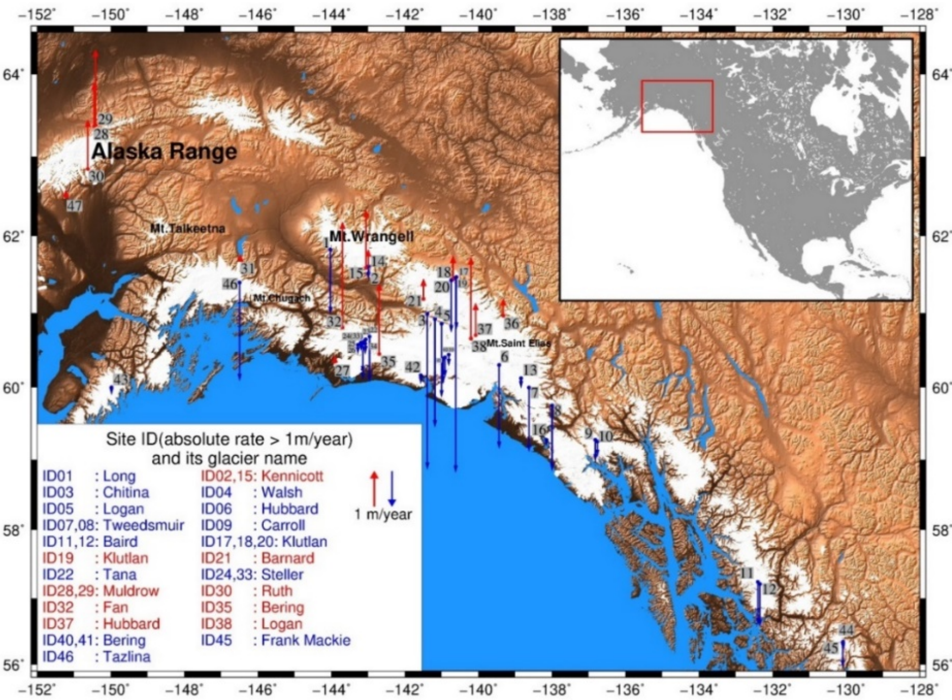

Figure 9. Rates of glacier elevation change from J2 over 2008–2016. Red (blue) arrows show positive (negative) rates. The inserted chart shows the site IDs and glacier names with absolute rates > 1 m/year (see Table A1).

Klutlan Glacier (Figure 10) is located in the St. Elias Mountains and has experienced repeated surges during the past hundreds of years (*Wright*, 1980) and in recent times (*Altena et al.*, 2019). Thus, this glacier is highly dynamic. Four Sites (Sites 17, 18, 19 and 20 in Figure 10) are near the terminus of Klutlan Glacier. At Sites 17 and 20, the rates of elevation change are about -3 m/yr, but the rate at Site 18 is much larger, reaching -11 m/yr. Potential causes of the large thinning rate at Site 18 and the positive rate at Site 19 (1.32 m/yr) can be explained as follows. A large tributary joins Klutlan Glacier near Sites 19 and 20. At the junction of glaciers, debris flows from the tributary have deposited near Site 19 to raise the elevations. Furthermore, between Sites 18 (altitude 1260 m) and 17 (altitude 1237 m), there is a nunatak at an altitude of about 1320 m. Site 17 is located in the northern side of the nunatak and is less affected by glacier surges. Thus, the presence of the nunatak results in a large difference between the rates at Site 17 and 18. Although the glacier thinning rates at Site 17 and Site 20 are close, the thinning patterns at the two sites are different. The annual variation of glacier elevation changes at Site 20 are much larger than that at Site 17.

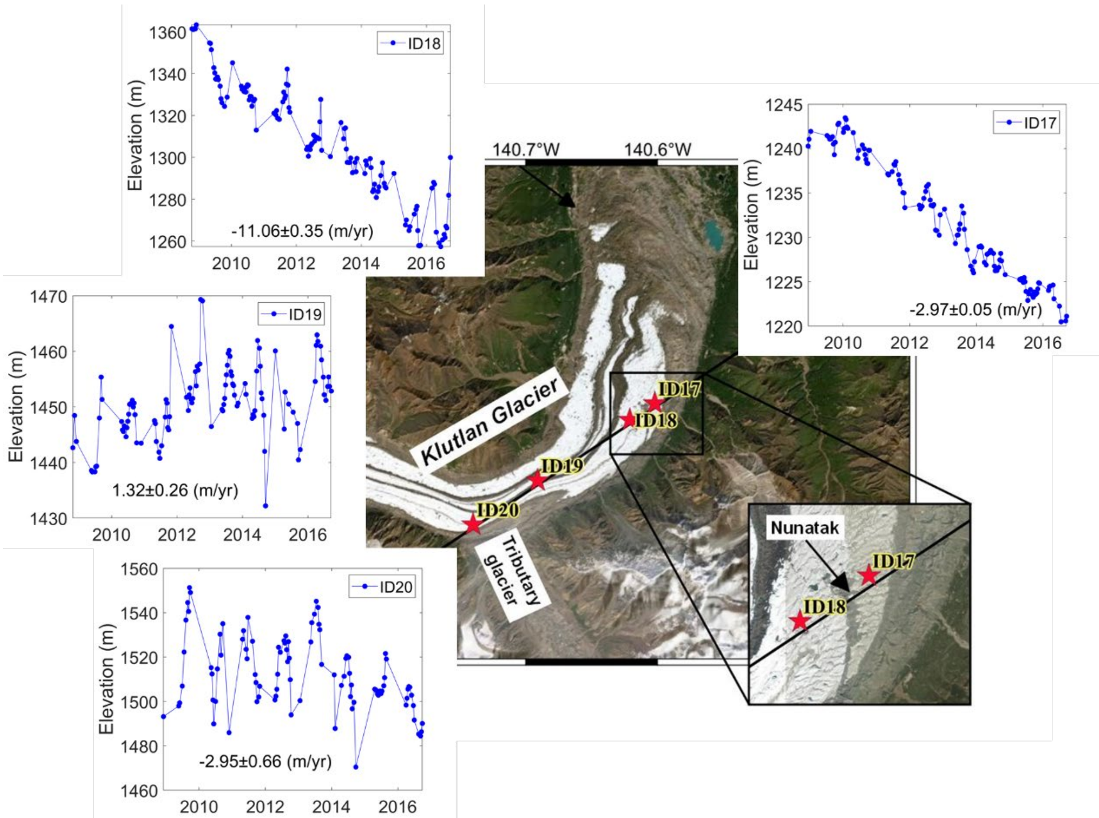

Figure 10. Glacier elevation changes at Sites 17, 18, 19 and 20 near Klutlan Glacier

Kennicott Glacier is the largest glacier in the Wrangell Mountains, covered with continuous debris

(*Anderson et al.*, 2019). Figure 11 shows the J2-derived elevation changes at Sites 2, 14 and 15 around this glacier. The elevations experience seasonal fluctuations with rapid increases in the thickness of glacier increases in spring and summer, and decreases in autumn and winter. Compared with the terrains in the upstream tributaries, the terrain around Sites 2 and 15 is flat. *Armstrong et al.* (2016) showed that, the glacier velocity of Kennicott in the early summer is the highest, and the velocity begins to slow down from autumn onward. The glacier growth in the lower reaches at Sites 2 and 15 should be mainly caused by the ice discharge from the upstream glaciers. At the same elevation zone, there are significant differences in the elevation change of the glaciers measured on different tributaries (*Das et al.*, 2014). The J2-derived declining rate of glacier elevations at Site 14 (-0.72 m/year) is larger than that of the entire Kennicott Glacier during 2000-2007 (*Das et al.*, 2014).

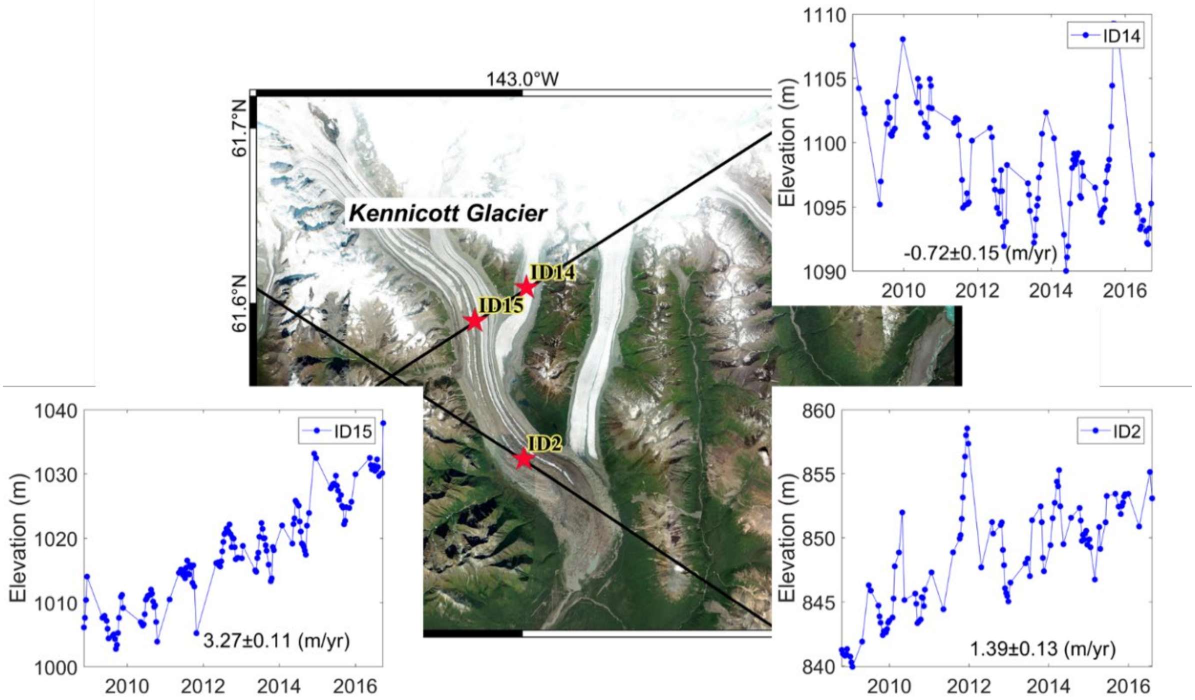

Figure 11. Glacier elevation changes at Sites 2, 14 and 15 near Kennicott Glacier

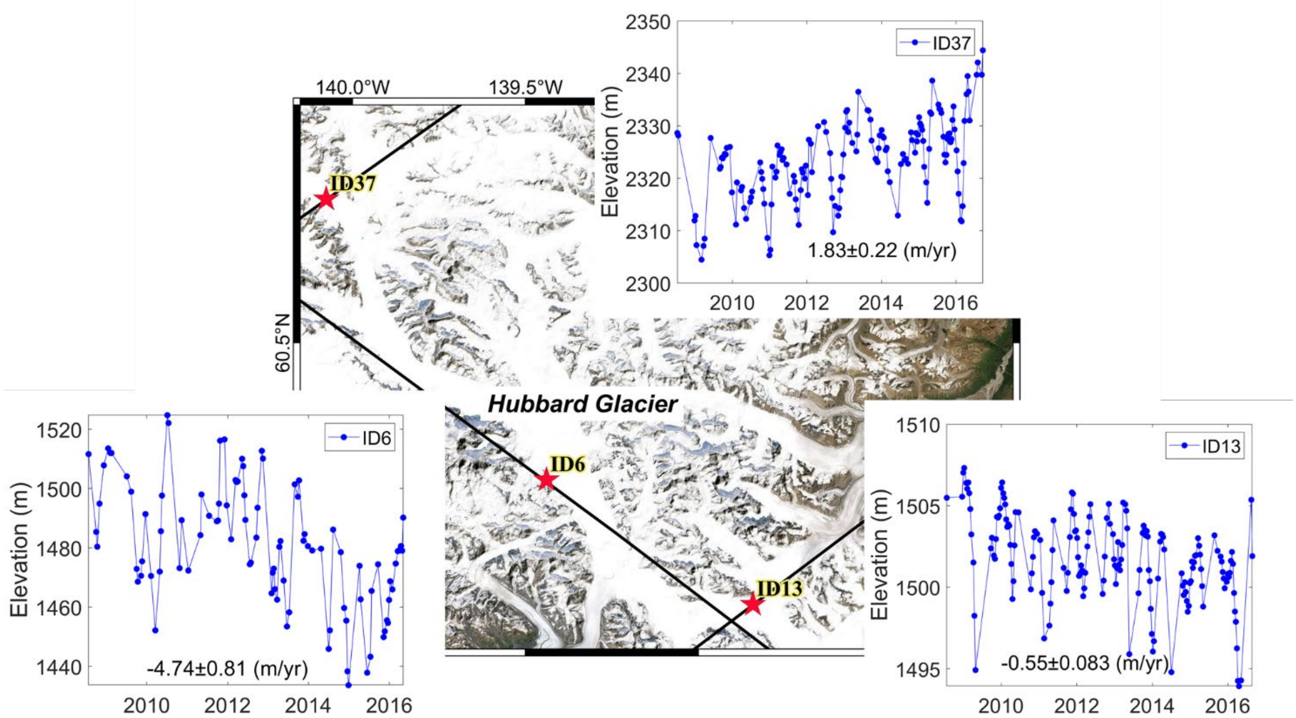

Figure 12. Glacier elevation changes at Sites 6, 13 and 37 near Hubbard Glacier

Hubbard Glacier is the largest temperate tidewater glacier spanning 123 km from North to South, and the glacier changes here are asynchronous with respect to the ice losses at its nearby glaciers (*Trabant et al.*, 2003a; *Stearns et al.*, 2015). Figure 12 shows that, the upstream of Hubbard Glacier thickened at a rate of 1.83 m/yr (Site 37), which was closely related to climate forcing (*Motyka and Truffer*, 2007; *Ritchie et al.*, 2008). In contrast to the previous understanding, the glacier elevations at the middle and lower reaches of Hubbard declined significantly (the rate at Site 6 is -4.74 m/yr), and the glaciers at the west end of Hubbard tend to thin slightly (the rate at Site 13 is -0.5 m/yr). The J2 results show a local variability of the glacier around Hubbard Glacier not reported in earlier studies.

Logan Glacier, Walsh Glacier and Chitina Glacier are tributaries of a large trunk that occupies the upper Chitina River Valley. More than 40 years ago, these glaciers and Anderson Glacier (next to Chitina Glacier) were connected to each other (*Ommanney*, 2002). In recent years, a large number of glaciers around this region have shrunk, leading to the retreats of glacier terminuses for up to tens of kilometers. As shown in Figure 13, the glacier elevations at Sites 3, 4 and 5 declined at the maximum rate of up to -8.82 m/yr at the terminuses). However, the glacier is thickening at Site 38, which is in the upper reaches of the Logan Glacier. These asynchronous glacier elevation changes are consistent with the measurements of *Larsen et al.* (2015). The measurements from T/P and J2 provide more details about the seasonal variations of the glacier fronts which are useful to the hydrological change research in the lower reaches of these glaciers. Due to the growth of glaciers at Logan Glacier's upstream (at Site 38), these three glaciers can sustain the water supply to the downstream river, despite the retreats of the terminuses of these three glaciers.

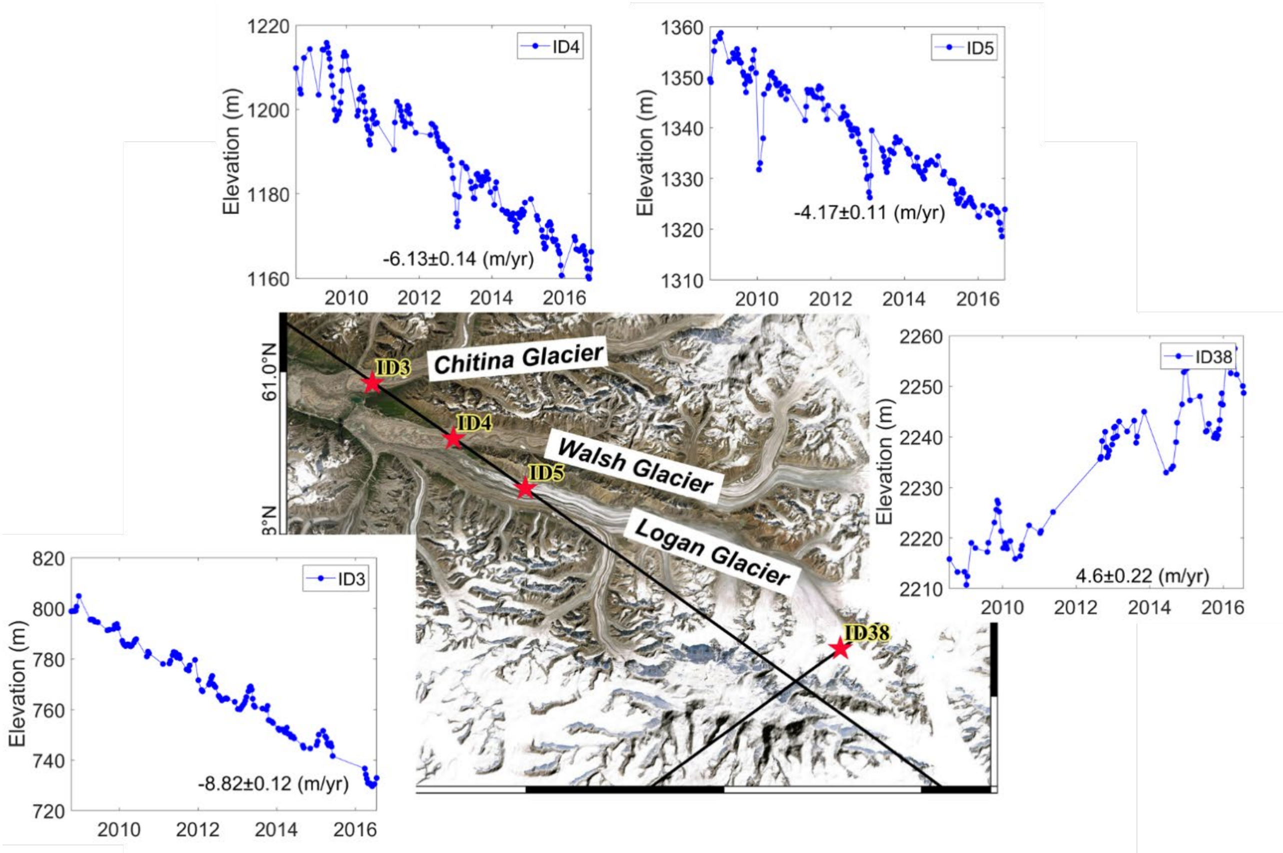

Figure 13. Glacier elevation changes at Sites 3, 4, 5 and 38 near Logan Glacier, Walsh Glacier, and Chitina Glacier

Steller Glacier and Waxell Glacier are located in the west of St. Elias Mountains. Figure 14 shows the glacier elevation changes at Sites 22, 23, 24, 33 and 34 over the west of Waxell Glacier and at Sites 25 and 26 near the upper reaches of Steller Glacier. The elevation changes suggest that the glaciers near Steller Glacier and Waxell Glacier were thinning with varying rates and their elevations experienced asynchronous interannual variations. A watershed divide between Waxell Glacier and

Steller Glacier results in two different drainage systems for the two glaciers (*Beedle et al.*, 2008). Waxell Glacier contributes to the surging Bering Glacier system, while Steller Glacier advances to the downstream Steller lobes along the main trunk to the south (*Bruhn et al.*, 2010). Compared with the rapid ice loss of Waxell Glacier, the interannual variation of Steller Glacier is relatively stable. This is consistent with the conclusion of (*Herzfeld and Mayer*, 1997). Site 27 is over an unknown frontal lake in the downstream of Steller Glacier. The elevations at Site 27 underwent distinct seasonal fluctuations and a trend reversal from a negative rate to a positive rate in late 2012. The seasonal fluctuations at Site 27 are reflected the variations in the stream flows originating from Steller Glacier.

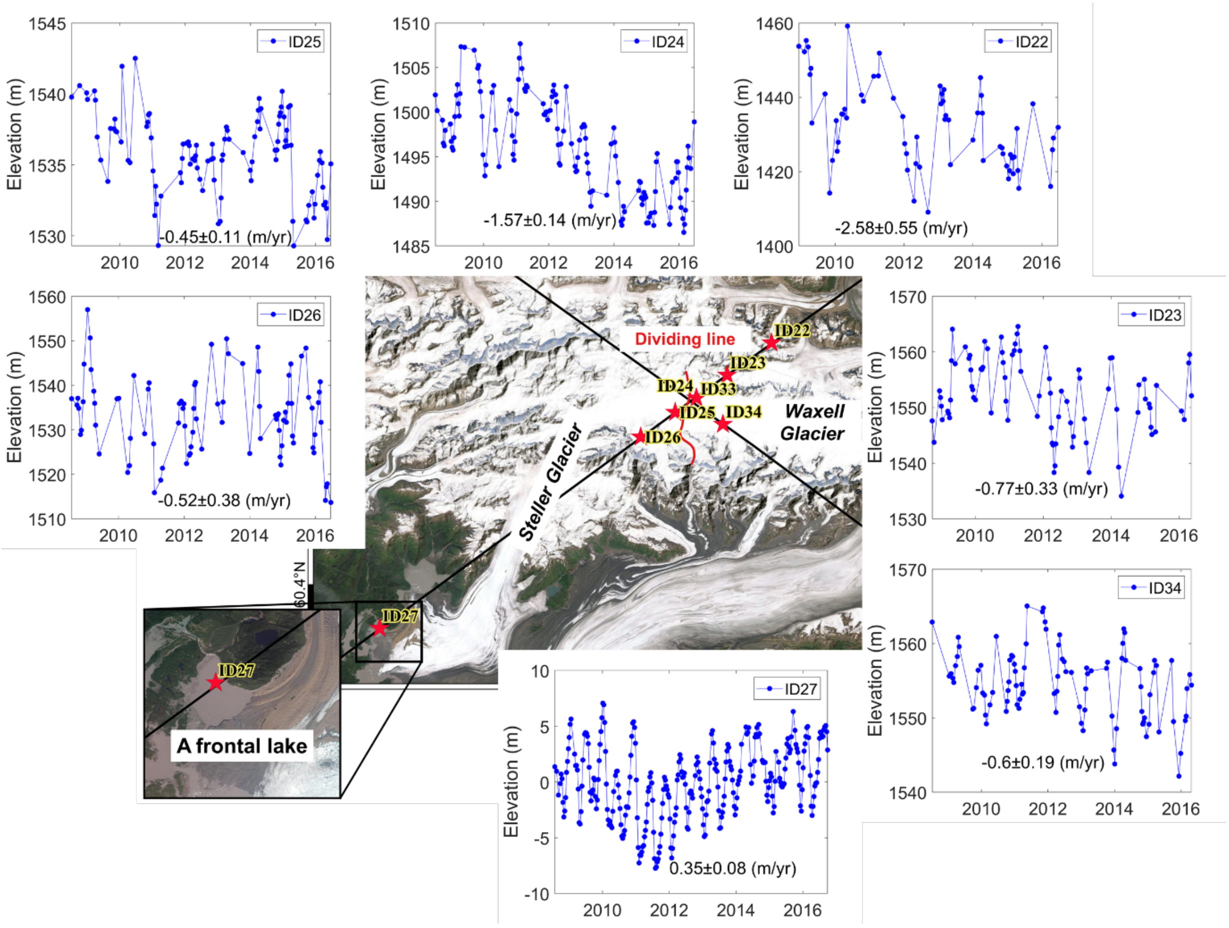

Figure 14. Glacier elevation changes at Sites 22, 23, 24, 25, 26, 27 and 34 near Steller Glacier and Waxell Glacier

The thickness of the accumulation zone of Tazlina Glacier can reach 1030 m, which is the thickest in Alaska glaciers (*Rignot et al.*, 2013). Figure 15 (Site 46) shows the elevation changes near an upper reach of Tazlina Glacier and its terminus (Site 31). Glaciers at Tazlina Glacier's upper reach thinned at a rate of -5.58 m/yr, but Tazlina's terminus gained mass at a rate of 0.26 m/yr (Site 31). The airborne Lidar measurements in the mid-1990s showed an average thinning rate of about -0.69 m/yr over Tazlina Glacier (*Molnia*, 2006), which is smaller compared to the rate at Site 46. Although J2 can only detect elevation changes at a single site (Site 31) over Tazlina Glacier's upper reaches, the large rate (-5.58 m/yr) suggests that the ongoing global warming may have accelerated glacier melt at Tazlina Glacier.

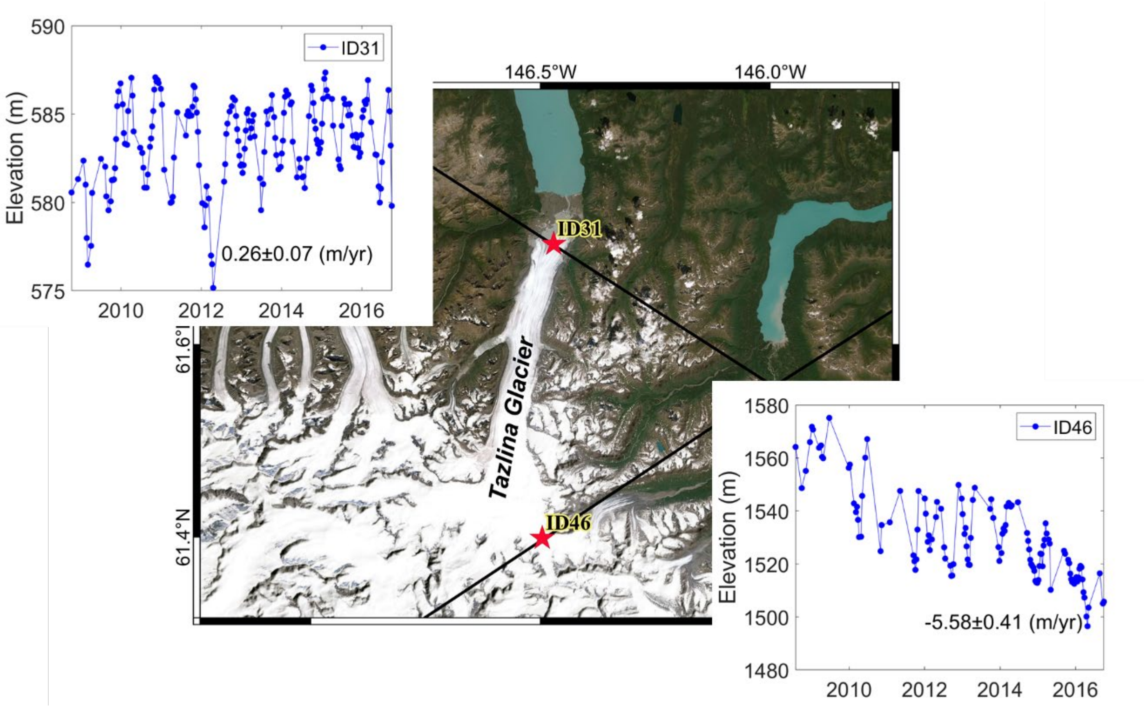

Figure 15. Glacier elevation changes at Sites 31 and 46 near Tazlina Glacier

Last, we discuss the J2-derived elevation changes over glaciers in the Central Alaska Range. Glaciers here have experienced rapid thinning and retreating in the early 2000s (*Adema et al.*, 2007). Figure 16 shows the glacier elevation changes from J2 at Sites 28, 29, 30 and 47 near Kahiltna Glacier, Ruth Glacier, and Muldrow Glacier around the Central Alaska Range. Instead of thinning, the glaciers at these sites were growing at rates ranging from 0.39 to 4.28 m/year. These rising glacier elevations indicate mass gains around the four sites. One explanation of the increased elevations at the lower reaches of the three glaciers is that the rapid melting of glaciers in the Central Alaska Range discharged more ice into the lower reaches. The excessive ice discharges accumulated and expanded the glaciers at the lower reaches due to basal roughness, bed topography and change in basin dimension (*Adema et al.*, 2007; *Molnia*, 2007; *Campbell et al.*, 2012; *Turrin et al.*, 2014).

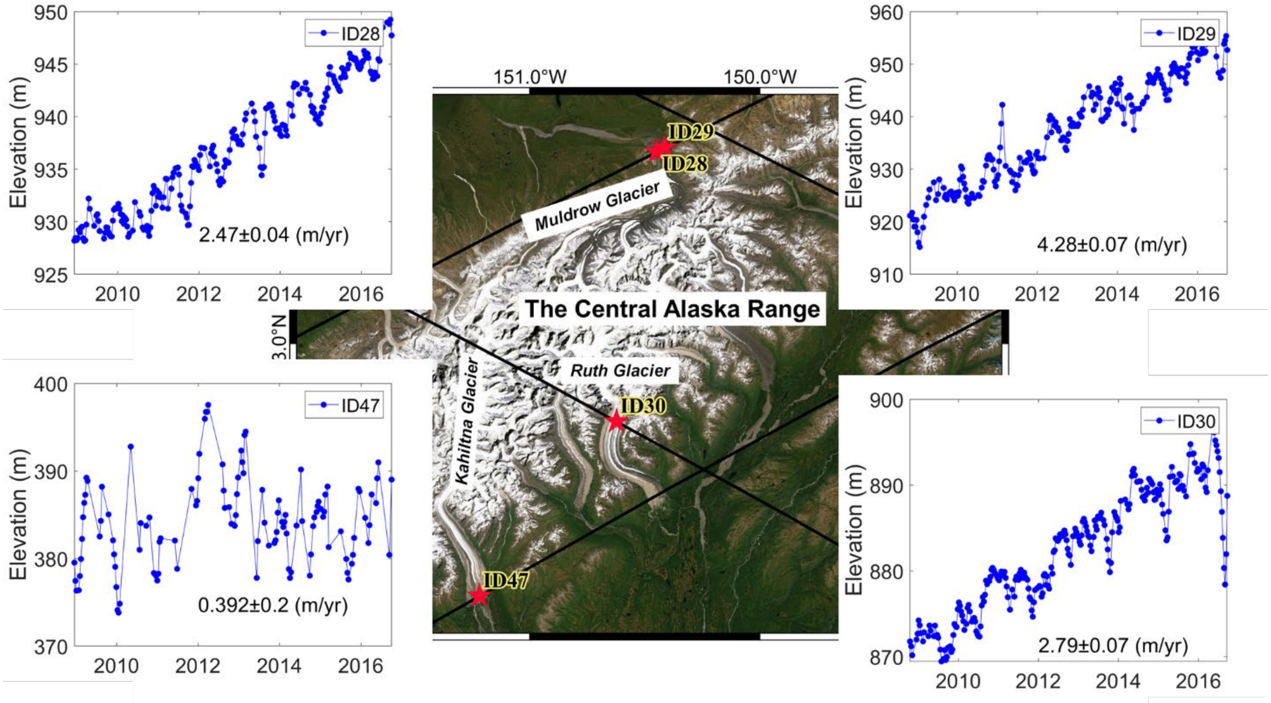

Figure 16. Glacier elevation changes at Sites 28, 29, 30 and 47 over the central Alaska Range

4.4 The response of glaciers to environmental changes

The types of glaciers at the 47 sites with the T/P and J2 elevation measurements include mountain glaciers, valley glaciers, tidewater glaciers, rock glaciers, among others. In the previous sections, we show the distinctive patterns of elevation changes associated with regional climates, orographic conditions, surface and substrate characteristics that might control the presences and evolutions of the studied glaciers. The altimeter result shows that neighboring glaciers can have asynchronous elevation change patterns. Below we examine various environmental factors that can cause such spatial and temporal changes in the glacier elevations.

First, we discuss the potential impact of the Pacific Decadal Oscillation (PDO) on Alaska glaciers. The PDO is a pattern of ocean-atmosphere climate variability, defined as the leading empirical orthogonal function of sea surface temperature (SST) anomalies over the North Pacific north of 20°N. In general, a positive phase of the PDO is associated with high precipitation and warming along the coast of Alaska and a negative phase leads to decreases in temperature and precipitation (*Arendt et al.*, 2009). During the study period (1992–2016), the phases of PDO underwent two notable shifts in 1998 and 2014 (Figure 17 a), respectively. The meteorological station records at the National Oceanic and Atmospheric Administration (NOAA, https://gis.ncdc.noaa.gov/maps/ncei) show that the impact of the PDO on annual winter precipitation and summer temperature in Alaska are spatially heterogenous. Specifically, the mountainous areas along the coast of Alaska experienced a significant decline in winter precipitation since 1999–2000 at the stations shown in Figure 17 b, c and d. As the PDO shifts from a negative phase to a positive in the summer 2014, the precipitation began to increase. However, the precipitation pattern on the northeast side of the Gulf of Alaska only shows stable, and small interannual fluctuation (Figure B1, a and b). At the stations near the Central Alaska Range (Figure 17 e, f and g), the summer temperature rose by a rate up to 0.061°C/year, compared to the negligible temperature change near Alaskan coastal areas (Figure B1, c and d).

The anticlockwise Alaska coastal current and the Alaska current (Figure 1) are responsible for the marine climate of the coast of Alaska (*Maraldo*, 2020). The ocean currents driven by strong wind, resulting in a large amount of precipitation on the windward side of the coastal mountains, especially in winter (2-6 m/yr) (*Weingartner et al.*, 2005). Due to the rain shadow effect, the heavy moisture stays on the windward side of the mountain, while the precipitation is rare on the leeward side. Since 1998, with the PDO phase changing from positive to negative, the precipitation along the coast of Alaska has experienced a distinct decline (Figure 17 b, c and d). The J2 result shows that the elevations of most glaciers in coastal mountainous area were rapidly declining (Table A2 and Table A3, Sites 13, 22, 24, 44, 45 and 46), or the glacier growth rates were slowing down significantly (Table A2 and Table A3, Sites 27 and 31). These changes in glacier elevations coincided with the significant decline of winter precipitation during this period (Figure 17 b, c and d). At the same time, the glacier elevations in the accumulation zone of Hubbard Glacier and Logan Glacier (Table A2 and Table A3, Sites 37 and 38) were increasing at a steady rate during the mission periods of T/P and J2. These glacier growths agree well with the estimates from surface mass balance (*Larsen et al.*, 2015) in the spatio-temporal pattern. For the thickening glaciers like Hubbard Glacier and Logan Glacier, the supply of new firn and refreezing processes play more dominant roles than climate change (*Trabant et al.*, 2003b).

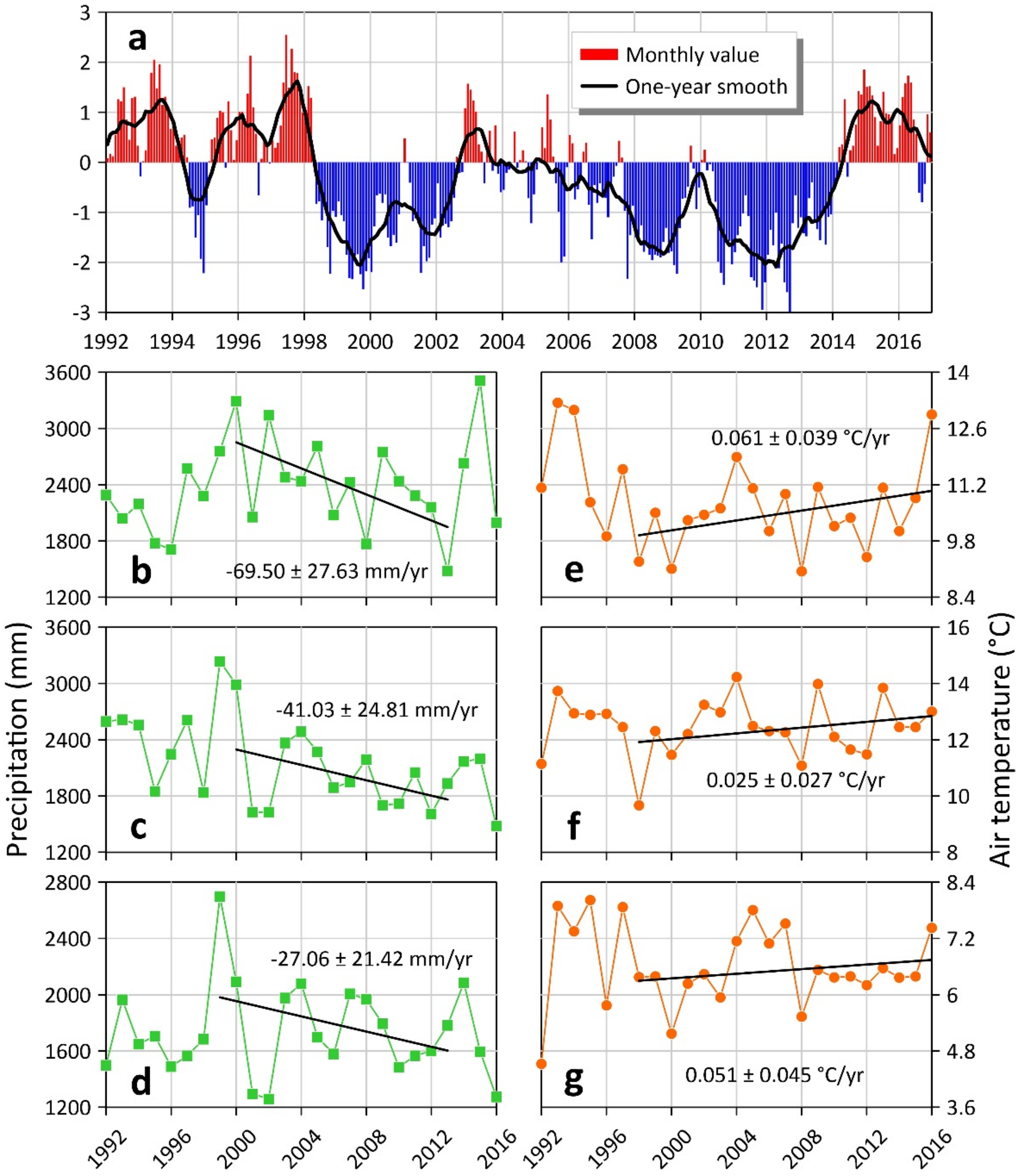

Figure 17. (a) The time series of Pacific Decadal Oscillation (PDO) from NOAA, and annual winter (October–April) precipitation changes in **(b)** Port San Juan, **(c)** Yakutat, and **(d)** Elfin Cove, and annual summer (May–September) temperature changes in **(e)** Chulitna River, **(f)** Puntilla, and **(g)** McKinley Park. The locations of meteorological stations are shown in Figure 1.

In the past half century, the temperature in the Central Alaska Range has increased by 3 °C, second only to that in northern Alaska (3.3 °C) (*Wendler et al.*, 2017). These above-average rises in temperature in Alaska are the result of the polar amplification of global warming (*Stone et al.*, 2002). Due to the large altitudinal range of Alaska, the glaciers here span a wide range of climate regimes, resulting in different responses of glaciers to different regional climate changes (*Young et al.*, 2018). For example, the cumulative mass balance recorded by the field sites indicate that Traleika Glacier, a major ice supply tributary at the upstream of Muldrow Glacier, experienced rapid ice loss, while the adjacent Kahiltna Glacier was growing slightly (*Adema*, 2006). Later, Kahiltna Glacier experienced ice loss, and by 2000 its mass balance was similar to that of Traleika Glacier (*Adema*, 2016). During our study period, a larger shift in rates of glacier elevation changes occurred in the Central Alaska Range (Site 28 and 47). In the T/P era (1993–2002), the terminuses of Muldrow Glacier and Kahiltna Glacier were thinning at rates of -6.43 ± 0.36 m/yr and -2.34 ± 0.35 m/yr, respectively, but the rates became positive in the J2 era (Muldrow Glacier: 2.47 ± 0.04 m/yr, Kahiltna Glacier: 0.39 ± 0.20 m/yr). The significant warming in the ablation season since 2000 (Figure 17 e, f, and g) may contribute to this sudden shift in the rates.

Unlike land-terminating glaciers, tidewater glaciers are very sensitive to SST variations (*Motyka et al.*, 2003; *Maraldo*, 2020). In this study, Sites 42 and 43 are near Guyot Glacier and Aialik Glacier, which are typical tidewater glaciers around the Gulf of Alaska. At the outlets of these two glaciers, SST rose by ~ 2 °C from 2008 to 2016, according to data from JPL at https://podaac.jpl.nasa.gov. Figure 18 compares the J2-derived glacier elevation changes and temperature changes (from) at Sites 42 and 43. From 2008 to 2016, the glacier elevations at Site 42 (near Guyot Glacier) dropped at a rate -0.53 m/year, and at Site 43 (near Aialik Glacier) the rate is -0.70 m/year. The elevations at the two glaciers are negatively correlated with summer SST changes with a 2-year lag. A significant rise of water temperature may be a driving factor for the recent collapse and retreat of these tidewater glaciers (Site 42: from early 2011 to late 2014, Site 43: from early 2011 to mid-2016). At present, we do not have enough evidence to explain this time lag. A hypothesis is that the native cycles and morphometric characteristics of tidewater glaciers, the depth and geometry of the fjords may have affected patterns of glacier elevation changes (*McNabb et al.*, 2015; *Brinkerhoff et al.*, 2017; *Maraldo*, 2020). Previous studies have shown that ocean forcing can lead to a stable retreat of calving glaciers (*Holland et al.*, 2008; *Motyka et al.*, 2011) and to a smaller retreat rate of nonclimatic-control tidewater glaciers than that of terrestrial glaciers (*Larsen et al.*, 2015; *Maraldo*, 2020). The altimeter result in this study shows large interannual variabilities of tidal glaciers and fast shifts in elevation patterns (e.g., glaciers at Sites 42 rose before 2011, then fell and rose again in 2014). These short to long-term glacier variabilities are observed from the 10-day repeat, usable T/P and J2 data, which may overcome the problems of underestimation or overestimation of the long-term trend of a tidewater glacier mass budget based on observations with a low temporal resolution (such as those from airborne Lidar or stereo imagery measurements).

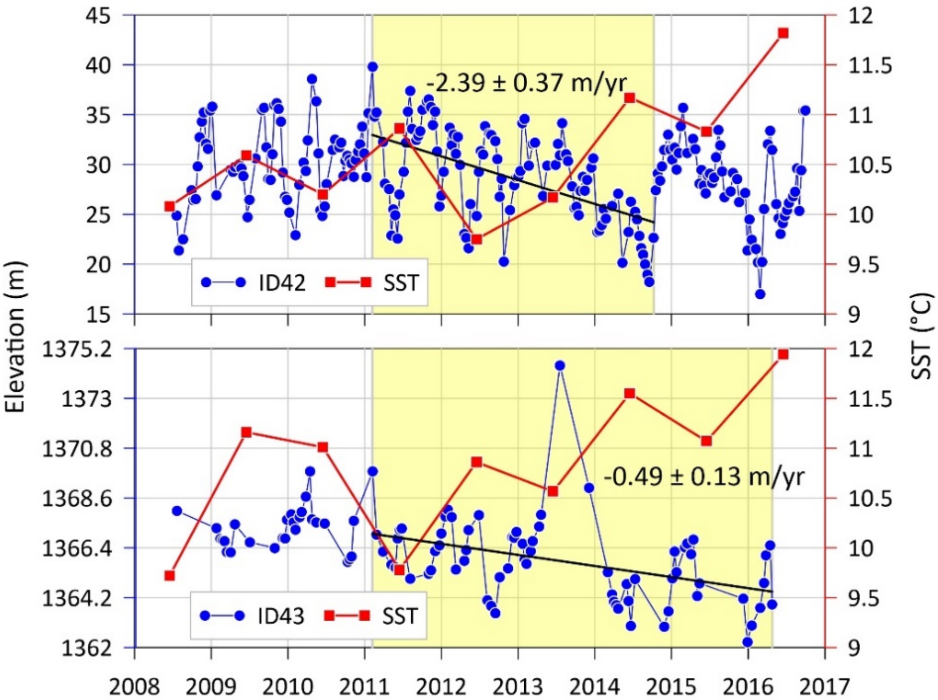

Figure 18. Glacier elevation changes at Site 42 and 43 (blue), and the annual summer (May–September) sea surface temperature (SST, red) near Sites 42 and43.

5 Conclusion

In the extreme terrain conditions of mountain glaciers, it is a challenge for satellite radar altimeters to monitor glacier elevation changes. In this study, we develop the GTM to extract glacier elevation changes based on the repeated and usable altimeter measurements. The GTM is an integrated processing system that includes the selection of the optimal waveform retracking algorithm, glacier footprint extraction, terrain correction and crossover analysis. An internal and external assessment confirm that the GIM can retrieve robust and precise glacier elevation changes over Alaska. The usable rates of the 10-day repeat altimeter observations range from 16% to 92%.

The T/P and J2 observations show that most glaciers in Alaska near the 47 sites in this study (1993–2016) are thinning. The maximum thinning rate reached -11.06 m/yr near Klutlan Glacier, followed by Chitina Glacier at -8.82 ± 0.12 m/year. Fan glacier has the largest rising rate of 5.99 ± 0.92 m/year, followed by Logan Glacier, which was rising at 4.30 m/year over 1993–2016. In addition, alternating rates in glacier elevation changes were also detected. Our result shows that that the thinning and thickening status of glaciers in St. Elias mountains are relatively stable in the two T/P–J2 periods, while larger rate shifts occurred over Muldrow Glacier, Kahiltna Glacier, Frank Mackie Glacier, Tazlina Glacier, and Kennicott Glacier.

With a phase change in the PDO in 1998 from positive to negative, a drop in winter precipitation for more than a decade occurred along the coast of Alaska. The precipitation drops in this area resulted in increasing glacier melts and slowed down the glacier growth rates in the accumulation zones. In the Central Alaska Range, the sharp increase in summer temperatures in 1998 intensified the long-term warming to accelerate glacier melts here. As a result, ice discharges from the mountains increased and then raised the elevations at the glacier terminuses, as evidenced by the altimeter observations. At two tidewater glaciers (Guyot Glacier and Aialik Glacier) in the Gulf of Alaska, we find that their interannual responses to summer SST anomalies are more significant than previously known. Warming waters may have increased their frontal ablations.

Despite the low spatial coverage of the T/P and J2 altimeters over Alaska mountain glaciers, the two missions' continuous 10-dy repeat and usable observations can provide information to better understand the short- and long-term complex dynamics of a mountain glacier if the glacier is sufficiently flat, wide and along a pass of the missions. The raw data from the T/P-series altimeter missions cannot be automatically used for detecting glacier elevation changes without a sophisticated processing system like the GTM. A capable altimeter processing system and repeat altimeter missions can facilitate the study of the physics of a small-scale glacier and provide data for verifying glacier measurements from other remote sensing technologies.

Acknowledgements

This study is supported by MOST/Taiwan under Grant Grants 109-2221-E-009-015-MY3 and 109-2611-M-009-001, and the National Natural Science Foundation of China (Grants 41974093 and 41774088). We are grateful to AVISO for the altimeter data used in this paper. All background images in Section 4.3 are from ESRI imagery.

References

Adema, G. W. (2006), Glacier monitoring in Denali National Park and Preserve, *Alaska Park Science*, *6*(2), 26-30.

Adema, G. W. 2016. Glacier Monitoring in Denali, Denali National Park & Preserve, Accessed on 21 April 2021, https://www.nps.gov/articles/denali-glacier-monitoring.htm.

Adema, G. W., R. Karpilo, and B. F. Molnia (2007), Melting Denali: effects of climate change on the glaciers of Denali National Park and Preserve, *Alaska Park Science*, *6*(1), 13-17.

Altena, B., T. Scambos, M. Fahnestock, and A. Kääb (2019), Extracting recent short-term glacier velocity evolution over southern Alaska and the Yukon from a large collection of Landsat data, *The Cryosphere*, *13*(3), 795-814.

Anderson, L. S., W. H. Armstrong, R. S. Anderson, and P. Buri (2019), Debris cover and the thinning of Kennicott Glacier, Alaska, Part B: ice cliff delineation and distributed melt estimates, *The Cryosphere Discuss.*, *2019*, 1-29, doi:10.5194/tc-2019-177.

Arendt, A., J. Walsh, and W. Harrison (2009), Changes of Glaciers and Climate in Northwestern North America during the Late Twentieth Century, *Journal of Climate*, *22*(15), 4117-4134, doi:10.1175/2009jcli2784.1.

Armstrong, W. H., R. S. Anderson, J. Allen, and H. Rajaram (2016), Modeling the WorldView-derived seasonal velocity evolution of Kennicott Glacier, Alaska, *Journal of Glaciology*, *62*(234), 763-777, doi:10.1017/jog.2016.66.

Becker, J., D. Sandwell, W. Smith, J. Braud, B. Binder, J. Depner, D. Fabre, J. Factor, S. Ingalls, and S. Kim (2009), Global bathymetry and elevation data at 30 arc seconds resolution: SRTM30_PLUS, *Marine Geodesy*, *32*(4), 355-371.

Beckley, B. D., N. Zelensky, S. Holmes, F. Lemoine, R. Ray, G. Mitchum, S. Desai, and S. Brown (2010), Assessment of the Jason-2 extension to the TOPEX/Poseidon, Jason-1 sea-surface height time series for global mean sea level monitoring, *Marine Geodesy*, *33*(S1), 447-471.

Beckley, B. D., N. P. Zelensky, S. B. Luthcke, and P. S. Callahan (2004), Towards a Seamless Transition from TOPEX/Poseidon to Jason-1, *Marine Geodesy*, *27*(3-4), 373-389, doi:10.1080/01490410490889148.

Beedle, M., M. Dyurgerov, W. Tangborn, S. Khalsa, C. Helm, B. Raup, R. Armstrong, and R. Barry (2008), Improving estimation of glacier volume change: a GLIMS case study of Bering Glacier System, Alaska, *The Cryosphere*, *2*(1), 33-51.

Berthier, E., E. Schiefer, G. K. Clarke, B. Menounos, and F. Rémy (2010), Contribution of Alaskan glaciers to sea-level rise derived from satellite imagery, *Nature Geoscience*, *3*(2), 92.

Brenner, A. C., R. Blndschadler, R. Thomas, and H. Zwally (1983), Slope-induced errors in radar altimetry over continental ice sheets, *Journal of Geophysical Research: Oceans*, *88*(C3), 1617-1623.

Brenner, A. C., J. P. DiMarzio, and H. J. Zwally (2007), Precision and accuracy of satellite radar and laser altimeter data over the continental ice sheets, *Ieee Transactions on Geoscience and Remote Sensing*, *45*(2), 321-331, doi:10.1109/TGRS.2006.887172.

Brinkerhoff, D., M. Truffer, and A. Aschwanden (2017), Sediment transport drives tidewater glacier periodicity, *Nature Communications*, *8*, doi:ARTN 90 10.1038/s41467-017-00095-5.

Brown, G. (1977), The average impulse response of a rough surface and its applications, *IEEE transactions on antennas and propagation*, *25*(1), 67-74, doi:10.1109/TAP.1977.1141536.

Bruhn, R. L., R. R. Forster, A. L. Ford, T. L. Pavlis, M. Vorkink, R. Shuchman, and E. Josberger (2010), Structural geology and glacier dynamics, Bering and Stellar Glaciers, Alaska, *Bering Glacier: interdisciplinary studies of Earth's largest temperate surging glacier*, 217-233, doi:10.1130/2010.2462(11).

Brun, F., E. Berthier, P. Wagnon, A. Kaab, and D. Treichler (2017), A spatially resolved estimate of High Mountain Asia glacier mass balances, 2000-2016, *Nature Geoscience*, *10*(9), 668-673, doi:10.1038/NGEO2999.

Campbell, S., K. Kreutz, E. Osterberg, S. Arcone, C. Wake, K. Volkening, and D. Winski (2012), Flow dynamics of an accumulation basin: a case study of upper Kahiltna Glacier, Mount McKinley, Alaska, *Journal of Glaciology*, *58*(207), 185-195, doi:10.3189/2012JoG10J233.

Ciracì, E., I. Velicogna, and S. Swenson (2020), Continuity of the mass loss of the world's glaciers and ice caps from the GRACE and GRACE Follow-On missions, *Geophysical Research Letters*, *47*(9), 1-11, doi:10.1029/2019gl086926.

Dabo-Niang, S., F. Ferraty, and P. Vieu (2007), On the using of modal curves for radar waveforms classification, *Computational Statistics & Data Analysis*, *51*(10), 4878-4890, doi:10.1016/j.csda.2006.07.012.

Das, I., R. Hock, E. Berthier, and C. S. Lingle (2014), 21st-century increase in glacier mass loss in the Wrangell Mountains, Alaska, USA, from airborne laser altimetry and satellite stereo imagery, *Journal of Glaciology*, *60*(220), 283-293, doi:10.3189/2014JoG13J119.

Davis, C. H. (1997), A robust threshold retracking algorithm for measuring ice-sheet surface elevation change from satellite radar altimeters, *Ieee Transactions on Geoscience and Remote Sensing*, *35*(4), 974-979, doi:10.1109/36.602540.

Dussaillant, I., E. Berthier, F. Brun, M. Masiokas, R. Hugonnet, V. Favier, A. Rabatel, P. Pitte, and L. Ruiz (2019), Two decades of glacier mass loss along the Andes, *Nature Geoscience*, *12*(10), 802-808, doi:10.1038/s41561-020-0639-5.

Flament, T., and F. Rémy (2012), Dynamic thinning of Antarctic glaciers from along-track repeat radar altimetry, *Journal of Glaciology*, *58*(211), 830-840, doi:10.3189/2012JoG11J118830.

Forsberg, R., L. Sorensen, and S. Simonsen (2017), Greenland and Antarctica Ice Sheet Mass Changes and Effects on Global Sea Level, *Surveys in Geophysics*, *38*(1), 89-104, doi:10.1007/s10712-016-9398-7.

Frappart, F., S. Calmant, M. Cauhopé, F. Seyler, and A. Cazenave (2006), Preliminary results of ENVISAT RA-2-derived water levels validation over the Amazon basin, *Remote Sensing of Environment*, *100*(2), 252-264, doi:10.1016/j.rse.2005.10.027.

Frappart, F., B. Legrésy, F. Nino, F. Blarel, N. Fuller, S. Fleury, F. Birol, and S. Calmant (2016), An ERS-2 altimetry reprocessing compatible with ENVISAT for long-term land and ice sheets studies, *Remote Sensing of Environment*, *184*, 558-581.

Fricker, H. A., and L. Padman (2012), Thirty years of elevation change on Antarctic Peninsula ice shelves from multimission satellite radar altimetry, *Journal of Geophysical Research: Oceans*, *117*(C2).

Fu, L.-L., and A. Cazenave (2000), *Satellite altimetry and earth sciences: a handbook of techniques and applications*, Elsevier.

Gardner, A. S., et al. (2013), A Reconciled Estimate of Glacier Contributions to Sea Level Rise: 2003 to 2009, *Science*, *340*(6134), 852-857, doi:10.1126/science.1234532.

Heid, T., and A. Kääb (2012), Repeat optical satellite images reveal widespread and long term decrease in land-terminating glacier speeds, *The Cryosphere*, *6*(2), 467-478, doi:10.5194/tc-6-467-2012.

Herzfeld, U. C., and H. Mayer (1997), Surge of Bering Glacier and Bagley Ice Field, Alaska: an update to August 1995 and an interpretation of brittle-deformation patterns, *Journal of Glaciology*, *43*(145), 427-434, doi:10.3189/s0022143000035012.

Holland, D. M., R. H. Thomas, B. De Young, M. H. Ribergaard, and B. Lyberth (2008), Acceleration of Jakobshavn Isbrae triggered by warm subsurface ocean waters, *Nature Geoscience*, *1*(10), 659-664, doi:10.1038/ngeo316.

Hwang, C., Y.-S. Cheng, J. Han, R. Kao, C.-Y. Huang, S.-H. Wei, and H. Wang (2016), Multi-Decadal Monitoring of Lake Level Changes in the Qinghai-Tibet Plateau by the TOPEX/Poseidon-Family Altimeters: Climate Implication, *Remote Sensing*, *8*(6), doi:10.3390/rs8060446.

Hwang, C., S.-H. Wei, Y.-S. Cheng, A. Abulaitijiang, O. B. Andersen, N. Chao, H.-Y. Peng, K.-H. Tseng, and J.-C. Lee (2021), Glacier and lake level change from TOPEX-series and Cryosat-2 altimeters in Tanggula: Comparison with satellite imagery, *Terrestrial, Atmospheric and Oceanic Sciences 32*, 1-20, doi:doi: 10.3319/TAO.2020.11.15.01.

Jacob, T., J. Wahr, W. T. Pfeffer, and S. Swenson (2012), Recent contributions of glaciers and ice caps to sea level rise, *Nature*, *482*(7386), 514-518, doi:10.1038/nature10847.

Kääb, A., E. Berthier, C. Nuth, J. Gardelle, and Y. Arnaud (2012), Contrasting patterns of early twenty-first-century glacier mass change in the Himalayas, *Nature*, *488*(7412), 495-498, doi:10.1038/nature11324.

Larsen, C. F. (2010), IceBridge UAF Lidar Scanner L1B Geolocated Surface Elevation Triplets, Version 1, updated 2020, *Boulder, Colorado USA. NASA National Snow and Ice Data Center Distributed Active Archive Center*, doi:10.5067/AATE4JJ91EHC.

Larsen, C. F., E. Burgess, A. A. Arendt, S. O'Neel, A. J. Johnson, and C. Kienholz (2015), Surface melt dominates Alaska glacier mass balance, *Geophysical Research Letters*, *42*(14), 5902-5908, doi:10.1002/2015gl064349.

Lee, H. (2008), Radar altimetry methods for solid earth geodynamics studies, Doctoral dissertation thesis, 1-170 pp, The Ohio State University.

Lee, H., C. Shum, K.-H. Tseng, Z. Huang, and H.-G. Sohn (2013), Elevation changes of Bering Glacier System, Alaska, from 1992 to 2010, observed by satellite radar altimetry, *Remote Sensing of Environment*, *132*, 40-48, doi:10.1016/j.rse.2013.01.007.

Lee, H., C. Shum, Y. Yi, A. Braun, and C.-Y. Kuo (2008), Laurentia crustal motion observed using TOPEX/POSEIDON radar altimetry over land, *Journal of Geodynamics*, *46*(3-5), 182-193, doi:10.1016/j.jog.2008.05.001.

Legresy, B., and F. Remy (1997), Surface characteristics of the Antarctic ice sheet and altimetric observations, *Journal of Glaciology*, *43*(144), 265-275, doi:10.3189/S002214300000321X.

Luthcke, S. B., A. A. Arendt, D. D. Rowlands, J. J. McCarthy, and C. F. Larsen (2008), Recent glacier mass changes in the Gulf of Alaska region from GRACE mascon solutions, *Journal of Glaciology*, *54*(188), 767-777, doi:10.3189/002214308787779933.

Luthcke, S. B., T. J. Sabaka, B. D. Loomis, A. A. Arendt, J. J. McCarthy, and J. Camp (2013), Antarctica, Greenland and Gulf of Alaska land-ice evolution from an iterated GRACE global mascon solution, *Journal of Glaciology*, *59*(216), 613-631, doi:10.3189/2013JoG12J147.

Maraldo, D. R. (2020), Accelerated retreat of coastal glaciers in the Western Prince William Sound, Alaska, *Arctic Antarctic and Alpine Research*, *52*(1), 617-634, doi:10.1080/15230430.2020.1837715.

Martin-Puig, C., E. Leuliette, J. Lillibridge, and M. Roca (2016), Evaluating the performance of Jason-2 open-loop and closed-loop tracker modes, *Journal of Atmospheric and Oceanic Technology*, *33*(11), 2277-2288, doi:10.1175/JTECH-D-16-0011.1.

Martin, T. V., H. J. Zwally, A. C. Brenner, and R. A. Bindschadler (1983), Analysis and retracking of continental ice sheet radar altimeter waveforms, *Journal of Geophysical Research: Oceans*, *88*(C3), 1608-1616, doi:10.1029/JC088iC03p01608.

McMillan, M., A. Muir, A. Shepherd, M. Roca, J. Aublanc, P. Thibaut, M. Restano, A. Ambrozio, and J. Benveniste (2019), Sentinel-3 Delay-Doppler altimetry over Antarctica, *The Cryosphere*, *13*(2), 709-722, doi:10.5194/tc-13-709-2019.

McNabb, R. W., R. Hock, and M. Huss (2015), Variations in Alaska tidewater glacier frontal ablation, 1985–2013, *Journal of Geophysical Research: Earth Surface*, *120*(1), 120-136, doi:10.1002/2014JF003276.

Menounos, B., R. Hugonnet, D. Shean, A. Gardner, I. Howat, E. Berthier, B. Pelto, C. Tennant, J. Shea, and M. J. Noh (2019), Heterogeneous changes in western North American glaciers linked to decadal variability in zonal wind strength, *Geophysical Research Letters*, *46*(1), 200-209, doi:10.1029/2018GL080942.

Molnia, B. F. (2006), Satellite image atlas of glaciers of the world: Alaska, *US Geological Survey Professional Paper*, 1-525.

Molnia, B. F. (2007), Late nineteenth to early twenty-first century behavior of Alaskan glaciers as indicators of changing regional climate, *Global and Planetary Change*, *56*(1-2), 23-56, doi:10.1016/j.gloplacha.2006.07.011.

Molnia, B. F. (2008), *Glaciers of North America-Glaciers of Alaska*, Geological Survey (US), doi:10.3133/pp1386K.

Motyka, R. J., L. Hunter, K. A. Echelmeyer, and C. Connor (2003), Submarine melting at the terminus of a temperate tidewater glacier, LeConte Glacier, Alaska, USA, *Annals of Glaciology*, *36*, 57-65, doi:10.3189/172756403781816374.

Motyka, R. J., and M. Truffer (2007), Hubbard Glacier, Alaska: 2002 closure and outburst of Russell Fjord and postflood conditions at Gilbert Point, *Journal of Geophysical Research Earth Surface*, *112*(F2), 1-15, doi:10.1029/2006JF000475.

Motyka, R. J., M. Truffer, M. Fahnestock, J. Mortensen, S. Rysgaard, and I. Howat (2011), Submarine melting of the 1985 Jakobshavn Isbrae floating tongue and the triggering of the current retreat, *Journal of Geophysical Research-Earth Surface*, *116*, doi:10.1029/2009jf001632.

Muskett, R. R., C. S. Lingle, J. M. Sauber, B. T. Rabus, and W. V. Tangborn (2008), Acceleration of surface lowering on the tidewater glaciers of Icy Bay, Alaska, USA from InSAR DEMs and ICESat altimetry, *Earth and Planetary Science Letters*, *265*(3-4), 345-359, doi:10.1016/j.epsl.2007.10.012.

Neal, E. G., E. Hood, and K. Smikrud (2010), Contribution of glacier runoff to freshwater discharge into the Gulf of Alaska, *Geophysical Research Letters*, *37*(6), doi:10.1029/2010GL042385.

Neumann, T. A., et al. (2019), The Ice, Cloud, and Land Elevation Satellite – 2 mission: A global geolocated photon product derived from the Advanced Topographic Laser Altimeter System, *Remote Sensing of Environment*, *233*, doi:10.1016/j.rse.2019.111325.

Ommanney, C. (2002), Glaciers of North America—Glacier of Canada: Glaciers of the Canadian Rockies, *Satellite Image Atlas of Glaciers of the World*.

Peacock, N. R., and S. W. Laxon (2004), Sea surface height determination in the Arctic Ocean from ERS altimetry, *Journal of Geophysical Research: Oceans*, *109*(C7), 1-14, doi:10.1029/2001JC001026.

Raney, R. K. (1998), The delay/Doppler radar altimeter, *Ieee Transactions on Geoscience and Remote Sensing*, *36*(5), 1578-1588, doi:10.1109/36.718861.

Remy, F., and S. Parouty (2009), Antarctic Ice Sheet and Radar Altimetry: A Review, *Remote Sensing*, *1*(4), 1212-1239, doi:10.3390/rs1041212.

Rignot, E., J. Mouginot, C. Larsen, Y. Gim, and D. Kirchner (2013), Low-frequency radar sounding of temperate ice masses in Southern Alaska, *Geophysical Research Letters*, *40*(20), 5399-5405, doi:10.1002/. 2013GL057452.

Ritchie, J. B., C. S. Lingle, R. J. Motyka, and M. Truffer (2008), Seasonal fluctuations in the advance of a tidewater glacier and potential causes: Hubbard Glacier, Alaska, USA, *Journal of Glaciology*, *54*(186), 401-411, doi:10.3189/002214308785836977.

Schröder, L., M. Horwath, R. Dietrich, V. Helm, M. R. Broeke, and S. R. Ligtenberg (2019), Four decades of Antarctic surface elevation changes from multi-mission satellite altimetry, *The Cryosphere*, *13*(2), 427-449.

Stearns, L. A., G. S. Hamilton, C. J. van der Veen, D. Finnegan, S. O'Neel, J. Scheick, and D. Lawson (2015), Glaciological and marine geological controls on terminus dynamics of Hubbard Glacier, southeast Alaska, *Journal of Geophysical Research: Earth Surface*, *120*(6), 1065-1081, doi:10.1002/2014JF003341.

Stone, R. S., E. G. Dutton, J. M. Harris, and D. Longenecker (2002), Earlier spring snowmelt in northern Alaska as an indicator of climate change, *Journal of Geophysical Research: Atmospheres*, *107*(D10), ACL 10-11-ACL 10-13.

Trabant, D. C., R. M. Krimmel, K. A. Echelmeyer, S. L. Zirnheld, and D. H. Elsberg (2003a), The slow advance of a calving glacier: Hubbard Glacier, Alaska, USA, *Annals of Glaciology*, *36*, 45-50, doi:10.3189/172756403781816400.

Trabant, D. C., R. March, and D. Thomas (2003b), Hubbard Glacier, Alaska: Growing and advancing in spite of global climate change and the 1986 and 2002 Russell Lake outburst floods, *US Geological Survey*, *907*, 786-7100, doi:10.3133/fs00103.

Trantow, T., and U. C. Herzfeld (2016), Spatiotemporal mapping of a large mountain glacier from CryoSat-2 altimeter data: surface elevation and elevation change of Bering Glacier during surge (2011-2014), *International Journal of Remote Sensing*, *37*(13), 2962-2989, doi:10.1080/01431161.

Turrin, J. B., R. R. Forster, J. M. Sauber, D. K. Hall, and R. L. Bruhn (2014), Effects of bedrock lithology and subglacial till on the motion of Ruth Glacier, Alaska, deduced from five pulses from 1973 to 2012, *Journal of Glaciology*, *60*(222), 771-781, doi:10.3189/2014JoG13J182.

Wang, L., C. K. Shum, F. J. Simons, B. Tapley, and C. L. Dai (2012), Coseismic and postseismic deformation of the 2011 Tohoku-Oki earthquake constrained by GRACE gravimetry, *Geophysical Research Letters*, *39*, 1-6, doi:10.1029/2012gl051104.

Weingartner, T. J., S. L. Danielson, and T. C. Royer (2005), Freshwater variability and predictability in the Alaska Coastal Current, *Deep-Sea Research Part Ii-Topical Studies in Oceanography*, *52*(1-2), 169-191, doi:10.1016/j.dsr2.2004.09.030.

Wendler, G., T. Gordon, and M. Stuefer (2017), On the precipitation and precipitation change in Alaska, *Atmosphere*, *8*(12), 253, doi:10.3390/atmos8120253.

Wingham, D. J., C. G. Rapley, and H. Griffiths (1986), New Techniques in Satellite Altimeter Tracking Systems, paper presented at Proceedings of the 1986 International Geoscience and Remote Sensing Symposium, ESA, Zurich.

Wingham, D. J., A. Shepherd, A. Muir, and G. Marshall (2006), Mass balance of the Antarctic ice sheet, *Philosophical Transactions of the Royal Society A: Mathematical, Physical and Engineering Sciences*, *364*(1844), 1627-1635.

Wingham, D. J., D. Wallis, and A. Shepherd (2009), Spatial and temporal evolution of Pine Island Glacier thinning, 1995–2006, *Geophysical Research Letters*, *36*(17), 1-5, doi:10.1029/2009GL039126.

Wouters, B., A. S. Gardner, and G. Moholdt (2019), Global Glacier Mass Loss During the GRACE Satellite Mission (2002-2016), *Frontiers in Earth Science*, *7*, 1-11, doi:10.3389/feart.2019.00096.

Wright, H. (1980), Surge Moraines of the Klutlan Glacier, Yukon Territory, Canada: Origin, Wastage, Vegetation Succession, Lake Development, and Application to the Late-Glacial of Minnesota, *Quaternary Research*, *14*(1), 2-18, doi:10.1016/0033-5894(80)90003-4.

Yang, Y., C. Hwang, H.-J. Hsu, E. Dongchen, and H. Wang (2012), A subwaveform threshold retracker for ERS-1 altimetry: A case study in the Antarctic Ocean, *Computers & Geosciences*, *41*, 88-98, doi:10.1016/j.cageo.2011.08.017.

Young, J. C., A. Arendt, R. Hock, and E. Pettit (2018), The challenge of monitoring glaciers with extreme altitudinal range: mass-balance reconstruction for Kahiltna Glacier, Alaska, *Journal of Glaciology*, *64*(243), 75-88, doi:10.1017/jog.2017.80.

Zemp, M., et al. (2019), Global glacier mass changes and their contributions to sea-level rise from 1961 to 2016, *Nature*, *568*(7752), 382-386, doi:10.1038/s41586-019-1071-0.

Appendix A: Site IDs and rates of altimeter-derived glacier elevation changes

Table A1: Information about the 47 Sites with glacier elevation changes and glacier names

Site ID	Glacier name	Longitude, Latitude	Approximate altitude (m)	Approximate slope (degree)	T/P Pass number
1	Long	-144.026, 61.824	1133	0.7	2
2	Kennicott	-142.998, 61.511	749	0.5	2

3	Chitina	-141.389, 60.986	839	0.5	2
4	Walsh	-141.184, 60.918	1153	0.9	2
5	Logan	-141.002, 60.857	1383	3.1	2
6	Hubbard	-139.439, 60.304	1479	8.2	2
7	Tweedsmuir	-138.628, 59.997	1272	5.7	2
8	Tweedsmuir	-137.998, 59.754	327	1	2
9	Carroll	-136.823, 59.278	1150	3.4	2
10	Carroll	-136.766, 59.254	1089	0.1	2
11	Baird	-132.404, 57.24	1152	0.5	2
12	Baird	-132.345, 57.209	1204	1.1	2
13	Hubbard	-138.842, 60.125	1448	0	21
14	Kennicott	-142.995, 61.609	1131	3.6	47
15	Kennicott	-143.057, 61.59	991	1.3	47
16	——[a]	-138.152, 59.276	102	3.7	97
17	Klutlan	-140.602, 61.47	1237	0.1	123
18	Klutlan	-140.621, 61.464	1260	1.2	123
19	Klutlan	-140.691, 61.442	1353	0.6	123
20	Klutlan	-140.74, 61.426	1415	0.5	123
21	Barnard	-141.494,61.183	1366	0.5	123
22	Waxell	-142.963, 60.686	1316	4.1	123
23	Waxell	-143.07, 60.648	1660	4.9	123
24	Waxell	-143.144, 60.621	1520	0.7	123
25	Steller	-143.195, 60.604	1526	1.7	123
26	Steller	-143.278, 60.575	1587	0.1	123
27	——[b]	-143.907, 60.348	52	0.5	123
28	Muldrow	-150.449, 63.376	884	2	175
29	Muldrow	-150.414, 63.384	964	3.4	175
30	Ruth	-150.623, 62.846	854	0	180
31	Tazlina	-146.471, 61.704	680	0.5	180
32	Fan	-143.697, 60.806	1120	1.8	180
33	Waxell	-143.144, 60.621	1520	0.7	180
34	Waxell	-143.08, 60.59	1485	1.9	180
35	Bering	-142.697, 60.452	904	0.8	180

36	Kluane	-139.324, 60.963	1491	0.4	199
37	Hubbard	-140.076, 60.704	2235	0.5	199
38	Logan	-140.205, 60.659	2231	0.8	199
39	Seward	-140.808, 60.444	2097	2.4	199
40	Seward	-140.91, 60.407	2162	3.6	199
41	Bering	-140.963,60.388	2035	1.8	199
42	Guyot	-141.567, 60.165	48	4.7	199
43	Aialik	-149.98, 60	1334	0.4	206
44	Frank Mackie	-130.083, 56.343	529	0.5	223
45	Frank Mackie	-130.093, 56.336	575	5.7	223
46	Tazlina	-146.496, 61.399	1562	0	225
47	Kahiltna	-151.219, 62.498	320	0.1	251

[a]Nameless

[b]Site 27 is located on a frontal lake,

Table A2: Rates of glacier elevation change from T/P (1992-2002).

Site ID	**Elevation change rate (m/yr)**	**Usable data percentage (%)**	**Amplitude of annual change (m)**
13	-0.46 ± 0.29	19	1.54 ± 0.81
15	-2.06 ± 0.28	16	1.96 ± 1.16
16	-0.44 ± 0.39	21	5.07 ± 1.53
22	2.13 ± 0.43	40	3.6 ± 1.98
24	-0.64 ± 0.23	19	1.73 ± 0.89
25	-0.81 ± 0.17	19	0.92 ± 0.65
26	-4.51 ± 1.2	16	3.92 ± 4.82
27	0.5 ± 0.18	39	0.53 ± 0.79
28	-6.43 ± 0.36	29	4.24 ± 1.53
31	5.92 ± 0.3	50	0.39 ± 1.12
33	-0.43 ± 0.15	27	0.76 ± 0.64
34	-1.04 ± 0.15	35	1.77 ± 0.60
35	1.6 ± 0.24	21	2.56 ± 1.06

37	0.48 ± 0.21	45	1.98 ± 0.94
38	4.03 ± 0.31	24	4.06 ± 1.11
42	-0.48 ± 0.32	33	4.42 ± 1.26
44	13.19 ± 0.74	17	3.11 ± 3.41
45	11.33 ± 1.19	16	19.9 ± 5.44
46	1.82 ± 0.58	19	2.00 ± 2.34
47	-2.34 ± 0.35	26	6.59 ± 1.37

Table A3: Rates of glacier elevation change from J2 (2008-2016).

Site ID	Elevation change rate (m/yr)	Usable data percentage (%)	Annual amplitude (m)
1	-3.64 ± 0.53	30	7.53 ± 1.78
2	1.39 ± 0.13	34	0.32 ± 0.48
3	-8.82 ± 0.12	42	0.7 ± 0.38
4	-6.13 ± 0.14	56	1.06 ± 0.46
5	-4.17 ± 0.11	57	1.20 ± 0.38
6	-4.74 ± 0.81	31	2.51 ± 2.55
7	-3.64 ± 0.39	41	4.35 ± 1.43
8	-3.72 ± 0.42	30	2.05 ± 2.02
9	-1.21 ± 0.33	37	1.40 ± 1.34
10	-0.86 ± 0.06	23	0.80 ± 0.22
11	-2.43 ± 0.19	35	3.41 ± 0.71
12	-2.43 ± 0.33	43	3.29 ± 1.14
13	-0.55 ± 0.08	53	0.73 ± 0.29
14	-0.72 ± 0.15	36	2.01 ± 0.64
15	3.27 ± 0.11	46	0.98 ± 0.53
16	-0.35 ± 0.26	42	2.37 ± 0.91
17	-2.97 ± 0.05	40	0.49 ± 0.18
18	-11.06 ± 0.35	39	3.57 ± 1.54
19	1.32 ± 0.26	36	0.86 ± 0.82
20	-2.95 ± 0.66	31	12.52 ± 3.21
21	1.14 ± 0.65	23	6.39 ± 5.07

22	-2.58 ± 0.55	22	2.81 ± 1.91
23	-0.77 ± 0.33	27	1.25 ± 1.35
24	-1.57 ± 0.14	43	0.62 ± 0.65
25	-0.45 ± 0.11	35	0.43 ± 0.45
26	-0.52 ± 0.38	29	1.32 ± 1.23
27	0.35 ± 0.08	92	0.50 ± 0.27
28	2.47 ± 0.04	74	0.38 ± 0.15
29	4.28 ± 0.07	76	0.61 ± 0.25
30	2.79 ± 0.07	81	0.46 ± 0.24
31	0.26 ± 0.07	61	1.15 ± 0.24
32	5.99 ± 0.92	20	9.02 ± 3.20
33	-1.56 ± 0.09	48	0.59 ± 0.40
34	-0.60 ± 0.19	31	3.59 ± 0.74
35	3.99 ± 0.13	25	2.05 ± 1.23
36	0.97 ± 0.23	53	3.28 ± 0.72
37	1.83 ± 0.22	52	2.56 ± 0.74
38	4.60 ± 0.22	25	1.86 ± 0.76
39	-0.64 ± 0.19	33	1.44 ± 0.64
40	-1.13 ± 0.29	40	1.52 ± 1.06
41	-1.41 ± 0.33	48	1.60 ± 1.24
42	-0.48 ± 0.11	74	0.99 ± 0.38
43	-0.42 ± 0.07	31	0.48 ± 0.26
44	-0.49 ± 0.16	40	0.82 ± 0.59
45	-1.42 ± 0.29	34	2.93 ± 0.82
46	-5.58 ± 0.41	41	2.85 ± 1.29
47	0.39 ± 0.20	37	2.12 ± 0.70

Appendix B: Precipitations and temperatures

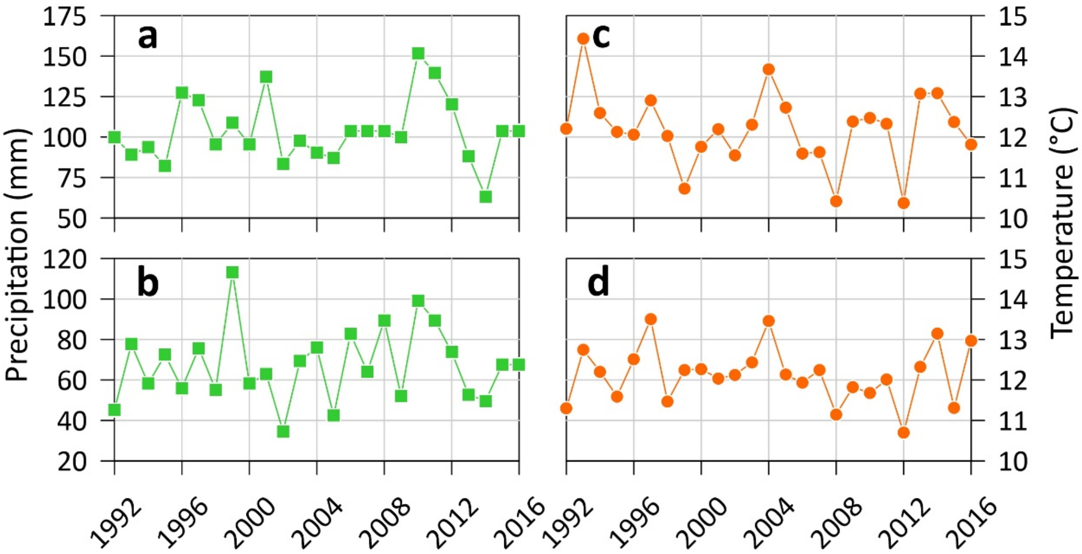

Figure B1: Annual winter (October–April) precipitation changes in **(a)** Beaver Creek, **(b)** Burwash, and annual summer (May–September) temperature changes in **(c)** Little Port Walter, and **(d)** Port San Juan. The locations of meteorological stations are shown in Figure 1. Note: when there are missing daily records (< 7 days), the values in this figure are linearly interpolated from neighboring values. If the time gap is more than 7 days, the missing values are from the monthly averages.